AD-A282 999

Development of Chemical-Vapor-Deposited Diamond for Infrared Optical Applications. Status Report and Summary of Properties

by

Daniel C. Harris
Research Department

JULY 1994

NAVAL AIR WARFARE CENTER WEAPONS DIVISION
China Lake, CA 93555-6001

DTIC
ELECTE
AUG 15 1994
S B D

Approved for public release; distribution is unlimited.

94 8 12 097

DTIC QUALITY INSPECTED 1

94-25609

Naval Air Warfare Center Weapons Division

FOREWORD

This report summarizes results of Navy contracts for the development of chemical-vapor-deposited optical quality bulk diamond from October 1990 through April 1993 and characterization through December 1993.

Work was carried out at Raytheon Research Division (Lexington, Mass., Contract N60530-90-C-0486), Texas Instruments (Dallas, Tx., Contract N60530-91-C0047), and Norton Company (Northboro, Mass., Contract N60530-91-C-0038). Raindrop impact testing and some mechanical testing was conducted by General Research Corporation (Santa Barbara, Calif., Contract N60530-92-C-0276). The project was sponsored by the Office of Naval Research and managed by the Optical and Electronic Materials Branch of the Chemistry Division of the Research Department.

This report was reviewed for technical accuracy by Kevin Gray, Tom Hartnett, John Trombetta, and Chuck Willingham.

Approved by
R. L. DERR, *Head*
Research Department
25 July 1994

Under authority of
D. B. McKINNEY
RAdm., U.S. Navy
Commander

Released for publication by
S. HAALAND
Deputy Commander for Research and Development

NAWCWPNS Technical Publication 8210

Published by ..... Technical Information Department
Collation ..... Cover, 32 leaves
First printing ..... 220 copies

REPORT DOCUMENTATION PAGE

Form Approved
OMB No. 0704-0188

Public reporting burden for this collection of information is estimated to average 1 hour per response, including the time for reviewing instructions, searching existing data sources, gathering and maintaining the data needed, and completing and reviewing the collection of information. Send comments regarding this burden estimate or any other aspect of this collection of information, including suggestions for reducing this burden, to Washington Headquarters Services, Directorate for Information Operations and Reports, 1215 Jefferson Davis Highway, Suite 1204, Arlington, VA 22202-4302, and to the Office of Management and Budget, Paperwork Reduction Project (0704-0188), Washington, DC 20503.

1. AGENCY USE ONLY *(Leave blank)*	2. REPORT DATE	3. REPORT TYPE AND DATES COVERED
	July 1994	Summary, Oct 1990-Dec 1993

4. TITLE AND SUBTITLE
Development of Chemical-Vapor-Deposited Diamond for Infrared Optical Applications. Status Report and Summary of Properties (U)

5. FUNDING NUMBERS
Project R534W54
Element 62234N

6. AUTHORS
Daniel C. Harris

7. PERFORMING ORGANIZATION NAME(S) AND ADDRESS(ES)
Naval Air Warfare Center Weapons Division
China Lake, CA 93555-6001

8. PERFORMING ORGANIZATION REPORT NUMBER
NAWCWPNS TP 8210

9. SPONSORING/MONITORING AGENCY NAMES(S) AND ADDRESS(ES)
Office of Naval Research
800 North Quincey Street
Arlington, VA 22217

10. SPONSORING/MONITORING AGENCY REPORT NUMBER

11. SUPPLEMENTARY NOTES

12a. DISTRIBUTION /AVAILABILITY STATEMENT
Approved for public release; distribution is unlimited.

12b. DISTRIBUTION CODE

13. ABSTRACT *(Maximum 200 words)*

(U) This report summarizes results of Navy contracts with Raytheon Research Division, Texas Instruments, and Norton Company for the development of chemical-vapor-deposited (CVD) optical-quality bulk diamond from October 1990 through April 1993 and characterization through December 1993. Clear windows with thicknesses of 0.3 to 1.0 millimeter (mm) and diameters up to 25 mm were produced. In the 8-to-14 micrometer (μm) infrared region, the absorption coefficient was as low as 0.1 to 0.3 cm(-1), optical scatter was below 1%, and emissivity was below 3% at 500°C for 0.5-to-1 mm thick samples. Microwave dielectric properties, thermal properties, and most mechanical properties of chemical-vapor-deposited diamond were equivalent to those of Type IIa natural diamond. The mechanical strength of 0.5-to-1 mm thick CVD diamond attained so far is an order of magnitude lower than that of natural diamond and is governed by microscopic cracks and defects.

14. SUBJECT TERMS
Diamond, Optical window, Optical properties, Mechanical properties, Thermal properties

15. NUMBER OF PAGES

16. PRICE CODE

17. SECURITY CLASSIFICATION OF REPORT	18. SECURITY CLASSIFICATION OF THIS PAGE	19. SECURITY CLASSIFICATION OF ABSTRACT	20. LIMITATION OF ABSTRACT
UNCLASSIFIED	UNCLASSIFIED	UNCLASSIFIED	UL

CONTENTS

Executive Summary 3

Why Diamond? 5

The Development Program 6
Before and After 7
Some Lessons Learned in Diamond Growth and Finishing 11

Interpreting the Infrared Spectrum of CVD Diamond 13
Hydrogen in CVD diamond 17

X-Ray and Microscopic Examination of Diamond Samples 20

Optical Characteristics 25
Background 25
Long-Wave Infrared Absorption 25
Long-Wave Infrared Emission 31
Optical Scatter 31
Refractive Index and Microwave Dielectric Properties 33
The Raman Spectrum of Imperfect Diamond Depends on Excitation Wavelength 36

Thermal Expansion and Thermal Conductivity 38

Mechanical Properties 41
Hardness, Modulus, Poisson's Ratio, and Toughness 41
Mechanical Strength 42
The Strength of Diamond is Governed by Flaw Size 48
Fine Polishing Has No Effect on the Strength of Diamond (Yet) 48
Waterjet Impact Resistance 51

References 57

Accession For
NTIS GRA&I ☑
DTIC TAB ☐
Unannounced ☐
Justification
By
Distribution
Availability Codes
Dist | Avail and/or Special
A-1

EXECUTIVE SUMMARY

This report summarizes results of Navy contracts with Raytheon Research Division (Lexington, Mass.), Texas Instruments (Dallas, Tx.), and Norton Company (Northboro, Mass.) for the development of chemical-vapor-deposited (CVD) optical-quality diamond windows from October 1990 through April 1993 and characterization through December 1993. At the outset of this effort, only modestly transparent CVD diamond had been made with thicknesses of tens of micrometers and 100 times too much absorption for Navy applications in the long-wave infrared (8 to 14 micrometer (μm)) region.

Deposition process development during this program yielded continuous progress in quality and scale and led to the production of approximately 50 clear windows with thicknesses of 0.3 to 1.0 millimeter (mm) and diameters up to 25 mm. Raytheon evaluated hot-filament and microwave plasma systems and chose the microwave system because it produced consistently higher optical quality diamond. Texas Instruments optimized a direct current plasma torch and Norton optimized growth of optical-quality diamond in a magnetically mixed arcjet. While all types of reactors could produce black diamond at high growth rates, optical-quality material demanded slow growth rates in the 1 to 5 μm/hour (h) range. Abrasive polishing with diamond grit was employed for optical finishing of flat windows.

By early 1993, high quality diamond was being produced with many properties comparable to those of Type IIa natural diamond. In the 8-14 μm infrared region, the absorption coefficient was as low as 0.1 to 0.3 centimeter $(cm)^{-1}$, optical scatter was below 1%, and emissivity was below 3% at 500°C for 0.5-to-1-mm-thick samples. Many of the best specimens had good visible transparency, as well as infrared transparency. The microwave dielectric properties, thermal conductivity, thermal expansion, hardness, toughness, and modulus of high quality chemical-vapor-deposited diamond were equivalent to the corresponding properties of Type IIa natural diamond. The mechanical strength of 0.5-to-1-mm-thick CVD diamond attained so far is an order of magnitude lower than that of natural diamond and is governed by microscopic cracks and defects. A comparison of properties of natural and CVD diamond is tabulated on the next page.

Comparison of Properties of Natural and CVD Diamond

Optical absorption coefficient @ 8-12 μm wavelength
- Gem diamond: 0.03-0.05 cm^{-1} @ 10.6 μm @ 20°C
- CVD diamond: 0.1-0.3 cm^{-1} @ 20°C

Absorption coefficient @ 8-12 μm is ~2x as great at 500°C as at 20°C

Emissivity @ 8-12 μm wavelength
- CVD diamond: 0.02 @ 300°C (sample thicknesses = 0.35-0.77 mm)
  0.03 @ 500°C (sample thicknesses = 0.35 mm)

Integrated forward optical scatter (There is no significant change in the range 20-500°C)
- Gem diamond: 0.2% (@ 0.63 μm integrated from 0.3 to 45°)
- (0.3-0.5 mm thick) 0.004% (@ 10.6 μm integrated from 1.1 to 45°)
- CVD diamond: 4% (@ 0.63 μm integrated from 2.5 to 70°)
- (0.35-0.77 mm thick) 0.2-0.8% (@ 10.6 μm integrated from 2.5 to 70°)

Microwave dielectric properties
- Gem diamond: Dielectric constant (ε) = 5.61 ±0.05; loss tangent = $(6 \pm 3) \times 10^{-4}$
- (@ 35 GHz) $100\Delta\varepsilon/\varepsilon_{18°C} = -0.026 + 0.006886T + 3.831\times10^{-7}T^2 + 1.185\times10^{-8}T^3$ (T=18-525°C)
- CVD diamond: Dielectric constant = 5.7; loss tangent < 4×10^{-4} (@ 35 GHz)

Thermal conductivity
- Gem diamond: ~23 W/cm·K @ 20°C; $k\ (W/cm\cdot K) = 2.833 \times 10^4/T^{1.245}$ (T = 500-1200 K)
- CVD diamond: ~20 W/cm·K @ 20°C

Thermal expansion coefficient
- Gem diamond: 0.9 ppm/K @ 0°C; 2.7 ppm/K @ 250°C

$\alpha = (1/L)dL/dT = 0.8345 + 9.174 \times 10^{-3}\ T - 7.828 \times 10^{-6}\ T^2 + 2.866 \times 10^{-9}\ T^3$ (T = 100-1600 K)

- CVD diamond: 1.1 ppm/K @ 0°C; 2.7 ppm/K @ 250°C

Hardness
- Gem diamond: 76-115 GPa (anisotropic)
- CVD diamond: 81 ±18 GPa (decreases by 30% at 800°C)

Fracture toughness
- Gem diamond: ~3.4 $MPa\sqrt{m}$
- CVD diamond: 5.3 ±1.3 $MPa\sqrt{m}$; 8 ±2 $MPa\sqrt{m}$

Young's modulus/Poisson's ratio
- Gem diamond: 1143 GPa/0.069 (average of anisotropic values)
- CVD diamond: Consistent with gem diamond value

Mechanical strength
- Gem diamond: ~3 GPa (tensile strength)
- CVD diamond: ~200-400 MPa (No loss of strength at 1000°C)
  (0.5-1 mm thick, polished disks tested with ring-on-ring flexure fixture; load radius = 4.88 mm, support radius = 8.61 mm)

Water jet damage threshold velocity

(0.8 mm diameter jet; 1-mm-thick, optical-quality diamond on solid backing)
- Gem diamond: ~530 m/s jet velocity
- CVD diamond: 200-250 m/s (central crazing); 350-500 m/s (circumferential crack)

WHY DIAMOND?

Infrared-transmitting window and dome materials for missiles and aircraft all suffer to some degree from insufficient resistance to rain and sand erosion and to thermal shock during rapid acceleration (Figure 1). While no material meets all demands, diamond offers the best known combination of physical properties for durability (Reference 1). Table 1 compares some properties of natural Type IIa diamond to those of sapphire and zinc sulfide. Sapphire is the most durable window material for the midwave (3 to 5 μm) atmospheric infrared transmission window and zinc sulfide is the material of choice for many long-wave (8 to 14 μm) applications (despite the fact that ZnS is limited to 8 to 10 μm) (Reference 2).

Infrared-transmitting dome at nose of missile protects seeker.

FIGURE 1. Dome at the Nose of a Missile Protects the Infrared Seeker. Domes can fail from rain and particle impact or from thermal shock induced by rapid acceleration.

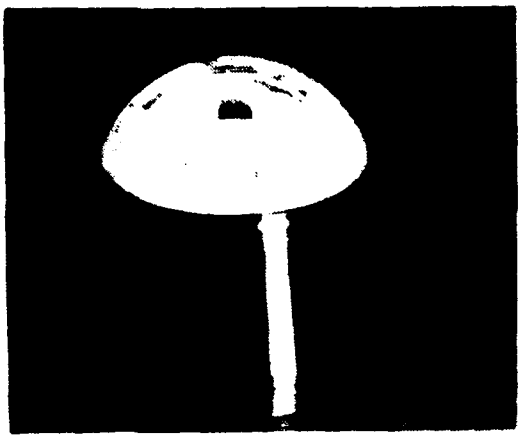

Thermal shock failure of dome from rapid acceleration.

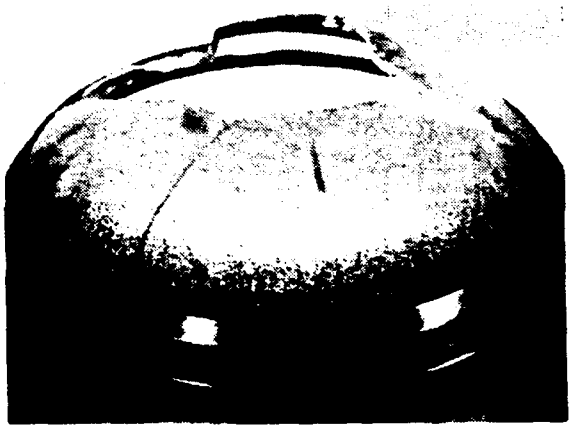

Rain impact failure during captive carry by airplane.

TABLE 1. Comparison of Properties of Infrared Window Materials at 25°C.

Properties	Type IIa Diamond	Zinc Sulfide	Sapphire
Hardness (kg/mm^2)	9000	230	1600
Fracture toughness ($MPa\sqrt{m}$), K_{Ic}	3.4	1.0	1.8
Strength (MPa), σ	~2500	~100	~700
Expansion coefficient (x 10^6, K^{-1}), k	1.0	7	6
Thermal conductivity (W/m-K), α	2000	19	34
Young's modulus (GPa), E	1143	74	344
Poisson's ratio, ν	0.07	0.29	0.27
Thermal shock figure of merit (R')[a] (kW/m)	4100	2.6	8.4
Dielectric Constant (35 GHz)	5.61	8.35	9.39 ($E \perp c$) 11.58 ($E \parallel c$)
Loss Tangent (35 GHz)	0.0006	0.0024	0.00005 ($E \perp c$) 0.00006 ($E \parallel c$)

[a] $R' = [\sigma(1-\nu)k]/(\alpha E)$. The greater the value of R', the greater the resistance to thermal shock. Properties in this table are strongly temperature-dependent.

Diamond is the hardest known material and has a high fracture toughness. It is therefore expected to be especially resistant to abrasion and erosion by dust and rain. The thermal conductivity of diamond is higher than that of copper. Coupled with its low thermal expansion and great strength, the thermal shock resistance of diamond exceeds that of ceramics by a factor of 100 to 1000. Diamond has an exceptionally wide optical window, spanning the ultraviolet, visible, infrared, millimeter and microwave regions. Millimeter-thick diamond is a good window for the 8- to 14-μm region, but weak absorption interferes with the 3- to 5-μm region. A thin coating of diamond, however, transmits adequately in both the 3- to 5- and 8- to 14-μm ranges. In contrast to most infrared window materials, diamond has a relatively low microwave dielectric constant that makes it suitable as a dual mode (infrared and microwave) aperture.

If diamond has an Achilles' heel, it is its limitation in high-temperature operations. Diamond is oxidized to carbon dioxide in the air at temperatures above 700°C (Reference 3). The thermodynamically stable phase of carbon at atmospheric pressure is graphite, not diamond. Even if it is protected from oxidation, diamond transforms spontaneously to graphite at temperatures above 1600°C (Reference 4).

THE DEVELOPMENT PROGRAM

The program to develop optical-quality CVD diamond was based on three primary contracts with Raytheon Research Division, Texas Instruments, and Defense Diamond Development Co. (a joint venture of Norton Co. and General Dynamics, hereafter referred

to as "Norton"). Work initiated late in 1990 resulted by early 1993 in diamond windows whose characteristics are described in this report. The goal for early 1993 was to produce flat, optically polished, transparent disks with a diameter of 20 mm and thickness of 1 mm. More than 50 disks with a thicknesses in the range 0.5 to 1 mm were received.

Three parallel efforts were undertaken to improve the probability of finding a method to produce high-quality diamond, which was by no means a certainty at the outset of this program. Raytheon's strategy was to explore hot-filament and microwave plasma deposition and to select one method for optimization after the first year. Texas Instruments chose to optimize a direct current torch, while Norton was optimizing a magnetically mixed arcjet.

BEFORE AND AFTER

During this effort, deposition technology advanced from producing black or dark gray diamond early in the program (Figure 2) to light gray or colorless diamond in 1993 (Figure 3). Improvements in infrared, visible and ultraviolet transmission are shown in Figures 4 and 5. Black diamond had negligible transmittance at wavelengths shorter than 3 μm and significant absorption and scatter in the long-wave infrared region (8 to 14 μm). The best colorless CVD diamond has nearly the same transmission as Type IIa natural diamond (lower trace of Figure 5).

FIGURE 2. Representative CVD Diamond Samples in 1991.

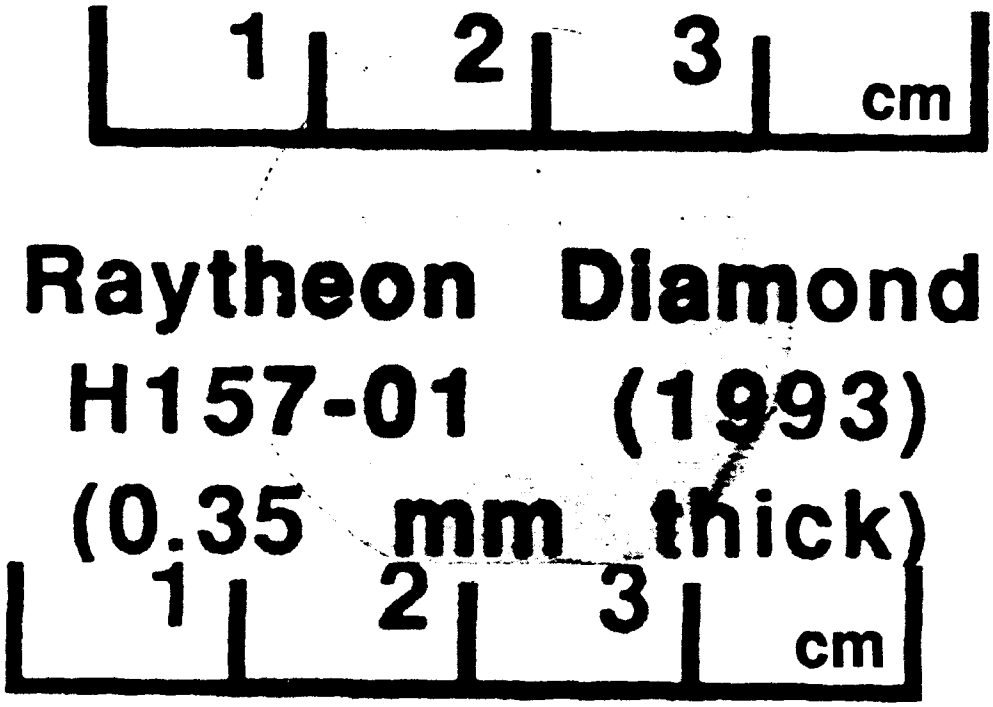

FIGURE 3. Highest-Optical-Quality CVD Diamond Samples in 1993.

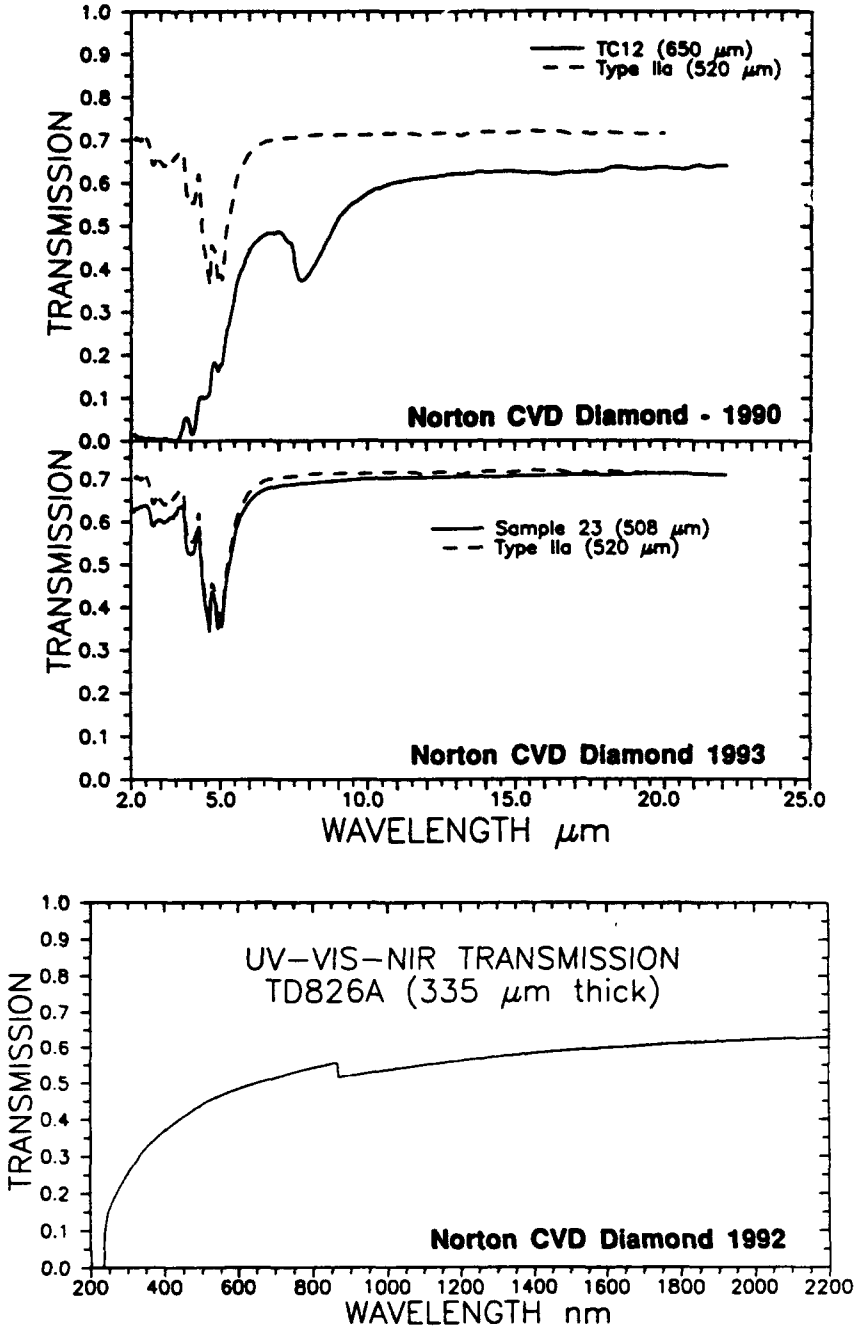

FIGURE 4. *Upper Spectrum* Compares Infrared Transmission of the Best Available Norton CVD Diamond in 1990 to That of Natural Type IIa Diamond. *Center spectrum* shows improvement in infrared transmission achieved by 1993. *Bottom spectrum* shows ultraviolet-visible-near infrared transmission of high-optical-quality Norton diamond. The discontinuity near 850 nanometers (nm) is an artifact.

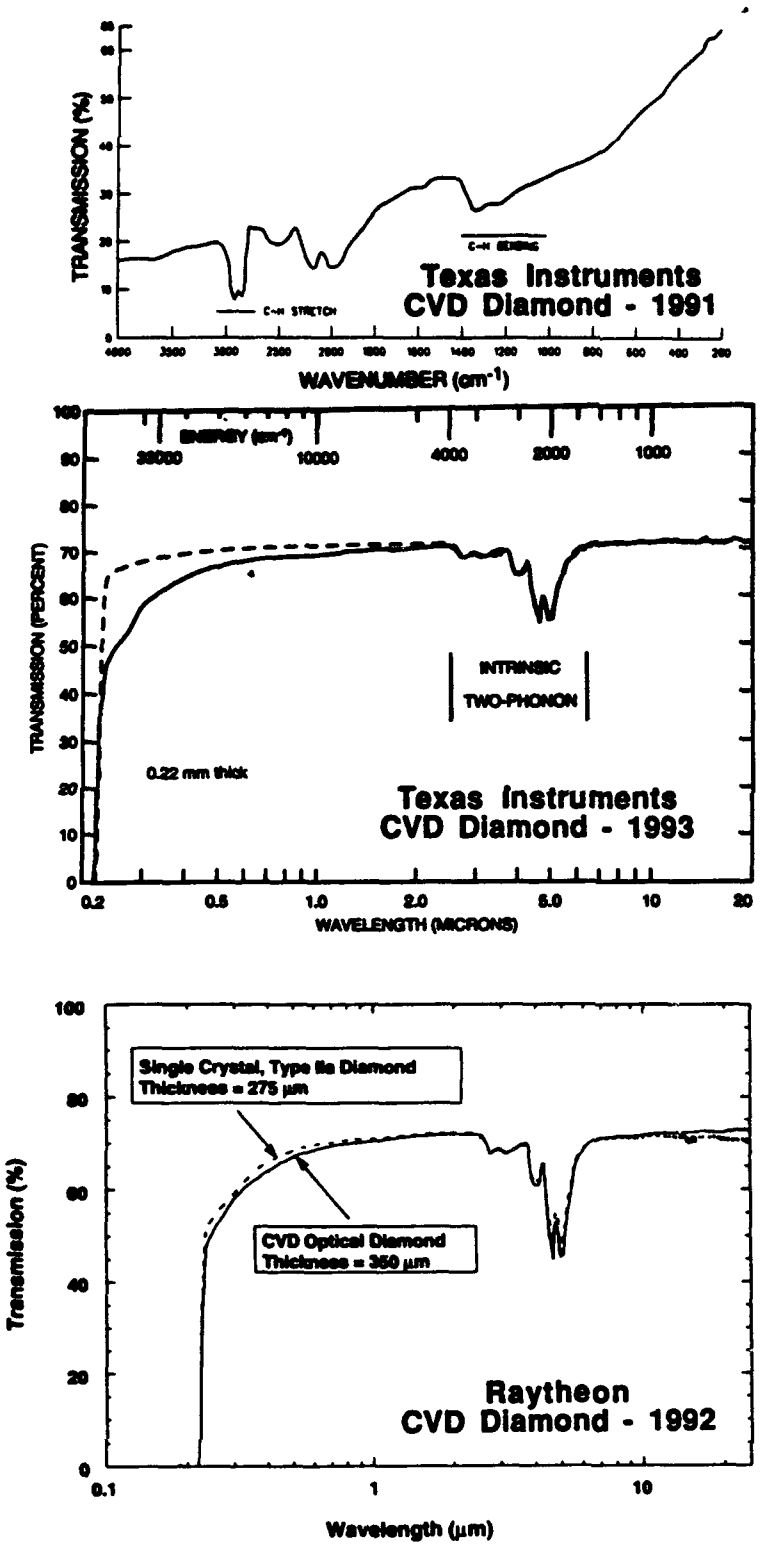

FIGURE 5. *Upper Spectrum* Shows Infrared Transmission of 0.58-mm-Thick CVD Diamond From Texas Instruments in 1991. Transmittance at 10 µm wavelength is ~30%. *Center spectrum* shows 0.22-mm-thick CVD diamond from Texas Instruments with transmission similar to that of natural Type IIa diamond through the ultraviolet, visible, and infrared ranges. *Bottom spectrum* shows excellent-optical-quality CVD diamond from Raytheon with transmission nearly identical to that of Type IIa diamond.

SOME LESSONS LEARNED IN DIAMOND GROWTH AND FINISHING

All three contractors found that (1) maximum growth rates were limited to 1 to 5 μm/h for optical quality material, (2) optical quality diamond grew in a highly stressed, macroscopically or microscopically cracked state, and (3) polishing was difficult because of diamond's extreme hardness. Growth rate is limited by the requirement for low methane concentration in the methane/hydrogen gas mixture. Higher growth rates are attained at higher methane concentration, but optical quality is not satisfactory at high methane concentration. It was challenging to grow 1-mm-thick optical quality material. High growth stress and low growth rates significantly reduced the probability of successful completion of a deposition run for thicknesses above 0.5 mm. Also, since surface roughness increases with increasing thickness (Figure 6), thicker diamond requires more material removal during polishing.

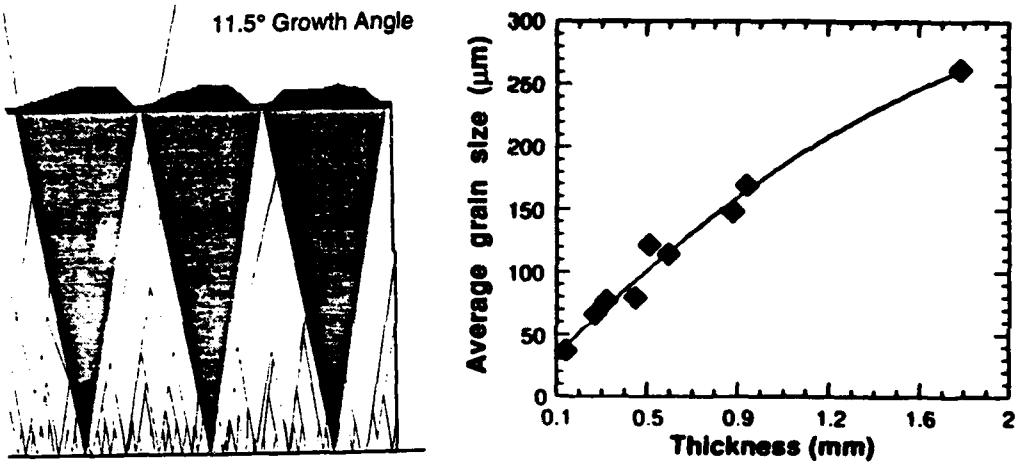

FIGURE 6. *Left:* Schematic Cross Section of CVD Diamond Showing Conical Grain Growth, With Large Grain Size at the Growth (upper) Surface and Small Grain Size at the Substrate (lower) Surface. *Right:* Measured grain size on growth surface as a function of thickness of diamond grown in microwave reactor at Raytheon.

All three contractors chose conventional high-speed lapping with diamond abrasive to polish CVD diamond wafers. Raytheon also pressed diamond against polished steel at 900-1100°C in an argon atmosphere for initial smoothing. Diamond dissolves in the metal under these conditions (Reference 5). Initial conditions for abrasive polishing of diamond are critical. There were numerous instances in which the workpiece was shattered because initial polishing was too aggressive.

Raytheon found that diamond grown by microwave plasma had better optical quality than diamond grown in a hot-filament reactor. Figure 7 shows the transmission of the highest quality diamond grown in a hot-filament reactor. The tantalum-tungsten alloy filament leaves ~10^{19} Ta atoms/cm^3 in the diamond (measured by secondary ion mass spectrometry), lowering the infrared transmission and thermal conductivity. Work with Pennsylvania State University (Reference 6) showed that heat transfer from the filament to the substrate is dominated by radiation from the filament and exothermic hydrogen atom

recombination on the growing diamond surface. System geometry, reactor pressure, and filament temperature are the most important factors determining the substrate temperature distribution.

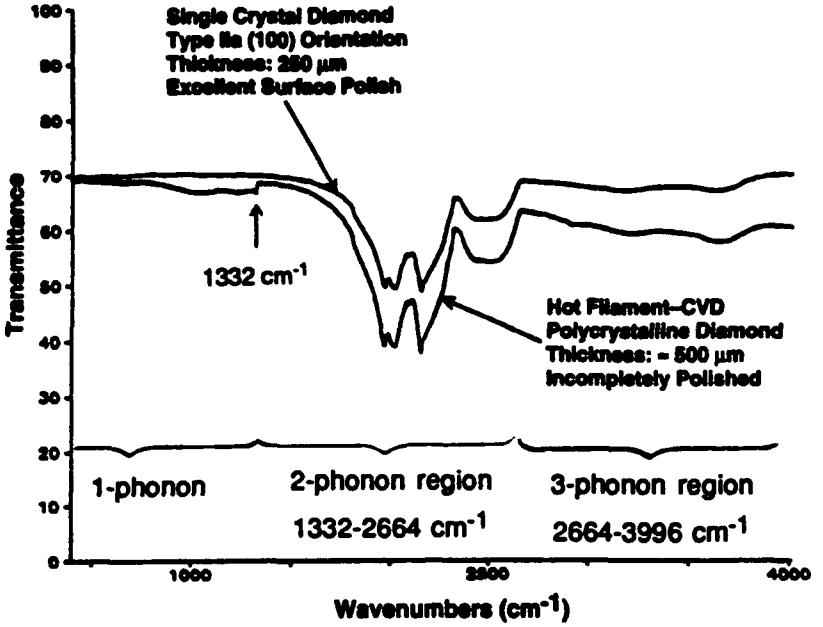

FIGURE 7. Infrared Transmission Spectrum of Highest-Quality Hot-Filament CVD Diamond From Raytheon. Note weak absorption in 1-phonon region from 1332 to ~900 cm^{-1}.

Two types of microwave reactors are in use at Raytheon for diamond deposition. A 5 kilowatt (kW) 2450 megahertz (MHz) unit manufactured by ASTEX (Woburn, Mass.) was modified at Raytheon. This instrument deposits 50-mm-diameter diamond plates with outstanding optical quality. A reactor capable of 125-mm-diameter deposition was designed and built at Raytheon with a 915 MHz microwave power source. The lower frequency gives a larger plasma ball capable of uniform growth over a larger area.

Norton observed boron and tungsten contamination in CVD diamond from component wear in their arcjet. Boron was eliminated by substituting nonboron-containing parts in the arcjet. Tungsten was reduced below levels detectable by x-ray fluorescence by redesign of part of the reactor.

To optimize operation of a direct current (dc) torch, Texas Instruments studied the effects of operating parameters on linear growth rate (µm/h), absorption by CH_2 groups near a wavelength of 3.4 µm, and optical scatter at a wavelength of 10 µm. (Measurement of absorption and scatter is described in the section Interpreting the Infrared Spectrum of Diamond.) The desired response is to maximize growth rate and minimize absorption and scatter. The absorption that we really wish to minimize is in the long-wave infrared region at 8 to 12 µm. The CH_2 absorption was chosen because it is correlated with long-wave absorption, but is easier to measure.

Properties were more dependent on temperature than on any other variable. For example, for a C-H stretching absorption coefficient of 1.0 cm^{-1}, it is necessary for temperature to be uniform to within ±3 K for the absorption coefficient to be uniform to within ±0.5 cm^{-1}. This is approximately a factor of ten greater temperature control than is currently available in some reactors. Allowable variations in hydrogen, methane, and oxygen flow and arc current were within easily attained limits.

INTERPRETING THE INFRARED SPECTRUM OF CVD DIAMOND

The infrared transmission spectrum of Type IIa natural diamond (the purest type of diamond) shown in Figure 7 is divided into regions labelled 1-phonon, 2-phonon, 3-phonon, etc. The highest vibrational frequency of the diamond crystal lattice involving one quantum of energy, called the zone-center mode, is observed near 1332 cm^{-1} in the Raman spectrum. This mode is forbidden by the infrared selection rules for a perfect diamond lattice and is not observed in the infrared spectrum of Type IIa diamond in Figure 7. However, weak 2-quantum transitions in the region 1332-2664 and weaker 3-quantum transitions in the region 2665-3996 cm^{-1} are allowed and observed in the infrared spectrum (Reference 7). In CVD diamond in Figure 7, weak absorptions are observed in the 1-phonon region because the perfect cubic symmetry of the lattice is broken by the presence of impurity atoms and defects such as vacancies and twin boundaries.

In the course of developing deposition methods for CVD diamond, it was necessary to interpret the transmission spectra of impure diamond with rough surfaces. Impurities absorb infrared radiation and activate 1-phonon absorptions of the diamond. Defects and grain boundaries produce some internal optical scatter, while rough surfaces create a great deal of optical scatter. How do we deconvolute scatter from absorption in CVD diamond?

Figure 8 illustrates the first two steps in this process. The upper spectrum shows the transmittance of well-polished Norton CVD diamond, with oscillations arising from constructive and destructive interference of light waves reflected between the two surfaces of the specimen. (Strong interference fringes were characteristic of most polished samples of Norton diamond, indicative of good polishing. Polished diamond from Raytheon and Texas Instruments had much weaker interference fringes. Unpolished diamond shows no fringes.) The first step in interpreting the spectrum of Norton diamond is to remove the fringes. This is done by taking the Fourier transform of the transmittance spectrum and removing the oscillation frequency. Additional noise can be filtered out by removing higher frequencies in the Fourier transform. The inverse Fourier transform of the filtered data gives the smooth spectrum shown by the dashed line in the upper spectrum and the solid curve in the lower spectrum of Figure 8.

The smooth spectrum is presumed to consist of intrinsic 2- and 3-phonon absorptions of diamond, plus impurity absorptions, plus broad optical scatter that increases as wavelength decreases. The curved, dashed baseline in the lower spectrum of Figure 8 is fit to the spectrum by matching three points where absorption is presumed to be negligible, near 2.5, 6.5, and 17.5 μm. (Absorption by Type IIa diamond is insignificant at these

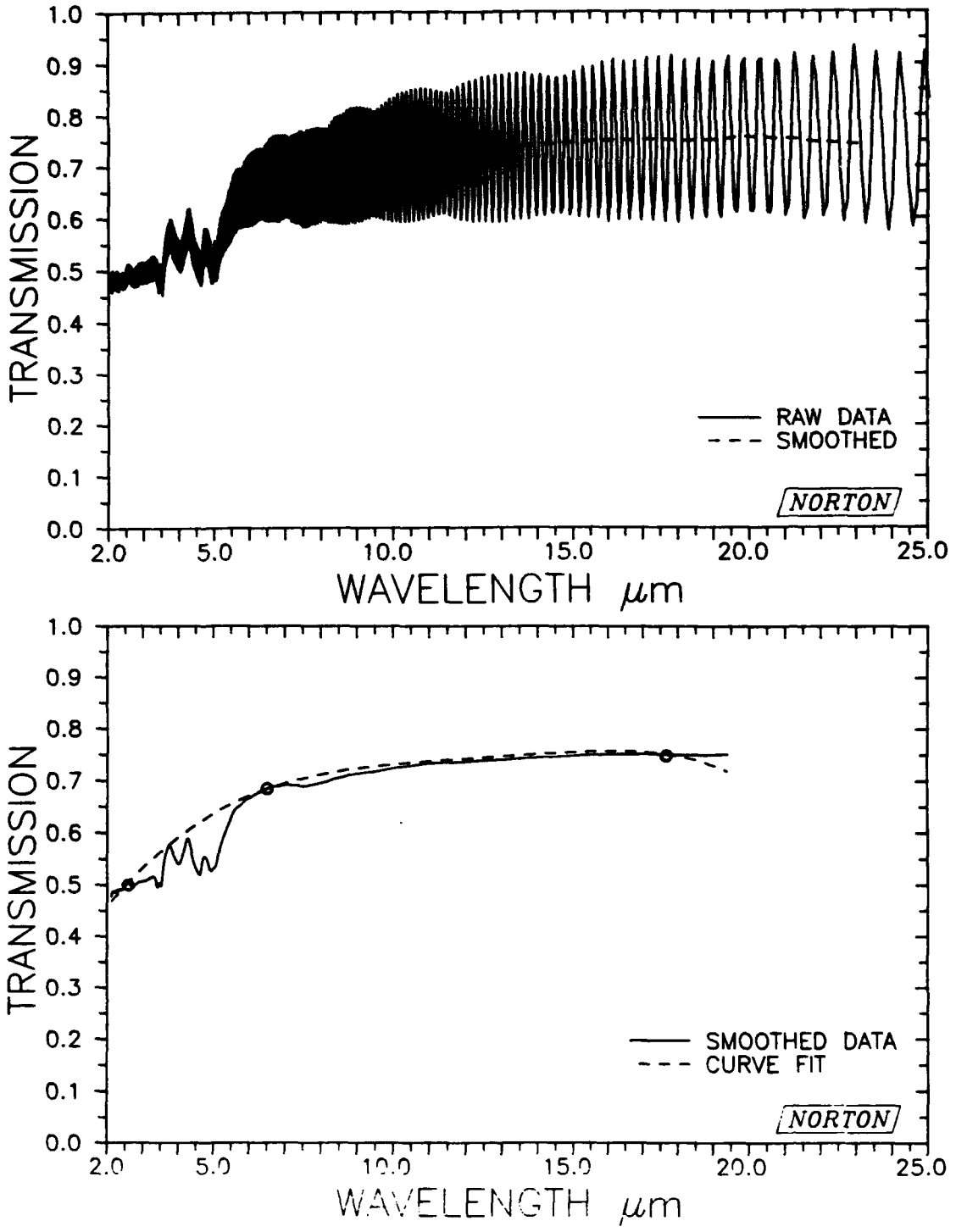

FIGURE 8. Upper Figure Shows Transmission Spectrum of Polished CVD Diamond From Norton Run TE29 Before (solid line) and After (dashed line) Fourier Filtering of Interference Oscillations. Dashed line in lower figure is cubic spline fit to three circle points in the smoothed spectrum. It is presumed that this fit represents the scattering baseline of the absorption spectrum.

wavelengths and impurities are not expected to absorb at these wavelengths.) The dashed curve is a cubic spline fit to these three points.

The upper part of Figure 9 shows a transmittance spectrum transformed into an absorption spectrum through the relation

$$\text{Extinction coefficient} = \beta = -\frac{1}{t}\ln\frac{T}{T_R} \qquad (1)$$

where t is the thickness of the specimen (cm), T is the measured transmittance in the smoothed spectrum (solid trace in the lower spectrum of Figure 8) and T_R is the theoretical transmittance of a diamond plate with no internal losses. T_R is determined by Fresnel reflection from the two surfaces and is given by

$$T_R = \frac{2n}{n^2+1} \qquad (2)$$

where n is the refractive index of Type IIa diamond. Taking n = 2.38 throughout the spectral range in Figure 9 gives T_R = 71.4%. That is, perfectly pure diamond is expected to transmit 71.4% in regions where there are no absorption bands.

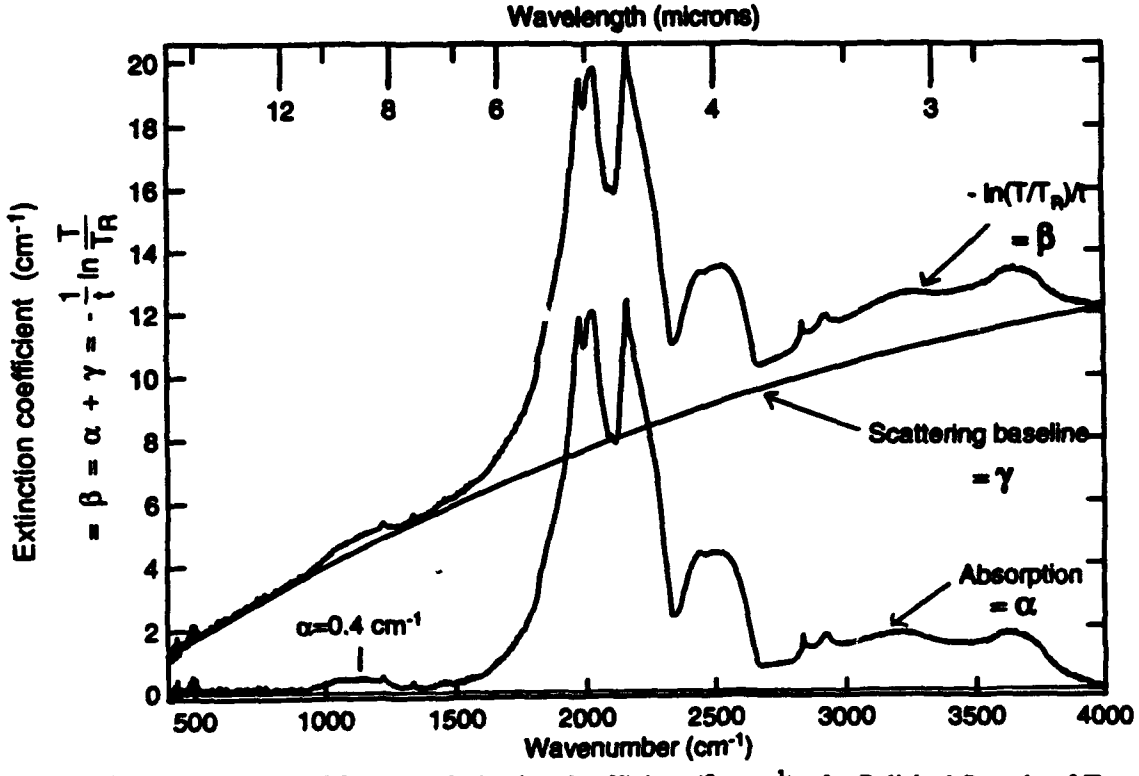

FIGURE 9. Upper Trace is Measured Extinction Coefficient (β, cm^{-1}) of a Polished Sample of Texas Instruments CVD Diamond. This is obtained from the transmission spectrum by computing $\beta = (1/t) \ln (T/T_R)$, where t is thickness, T is observed transmittance and T_R is theoretical transmittance (0.714). The scattering baseline (γ, cm^{-1}) fit to three points of this spectrum is also shown. When the scattering coefficient is subtracted from the extinction coefficient, the difference is the absorption coefficient (α, cm^{-1}).

The scattering baseline in Figure 9 corresponds to the dashed curve in the lower spectrum in Figure 8. When the scattering baseline is subtracted from the observed extinction spectrum, the absorption spectrum at the bottom of Figure 9 is left. This spectrum contains intrinsic absorptions of Type IIa diamond and extrinsic absorptions from impurities and defects. The ordinate is the absorption coefficient, α. The extinction coefficient is the sum of the absorption coefficient and a scattering coefficient, γ.

$$\underset{\text{extinction coefficient}}{\beta} = \underset{\text{absorption coefficient}}{\alpha} + \underset{\text{scatter coefficient}}{\gamma} \qquad (3)$$

Deconvolution of the infrared transmission spectrum into scatter and absorption components was validated at Texas Instruments. For samples with absorption coefficients in the range 0.2 to 2 cm^{-1}, laser calorimetry measurements were within experimental error of infrared transmission measurements. For one sample, whose scatter was estimated to be 19% based on transmission, direct measurements of forward and backward total integrated scatter at China Lake gave a sum of 16%.

To expedite deposition method development, Texas Instruments applied a coating with the same refractive index as diamond to unpolished CVD diamond. As shown in Figure 10, this removed most of the surface scatter and permitted infrared absorption to be measured without laborious polishing of the diamond.

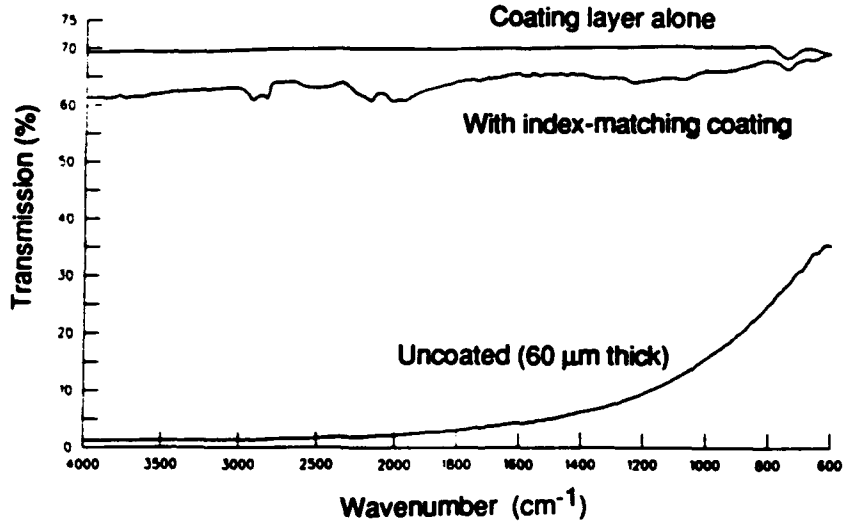

FIGURE 10. Lower Trace is Raw Transmission of Unpolished Texas Instruments CVD Diamond With a Thickness of 60 µm. Middle trace shows transmission after applying a thin coating that matches the refractive index of diamond. This coating eliminates most surface scatter. Upper trace shows transmission spectrum of coating layer alone, with thickness similar to that applied to diamond.

HYDROGEN IN CVD DIAMOND

Infrared spectra of early development samples of CVD diamond were dominated by strong C-H stretching absorption bands in the 2800-3000 cm^{-1} region. *Samples with strong C-H absorption invariably have strong absorption in the 1-phonon region* (~1000 to 1350 cm^{-1} in Figure 11). (Absorption in the 1-phonon region might arise from defect-activated 1-phonon diamond transitions or may be impurity absorptions.) It was therefore paramount to reduce the C-H content of CVD diamond to reduce long-wave infrared absorption. The middle and lower spectra in Figure 5 represent specimens in which there is negligible C-H absorption. The left side of Figure 12 shows the correlation between C-H absorption and hydrogen content for Texas Instruments dc plasma torch diamond, while the right side shows the correlation between C-H absorption and 1-phonon absorption.

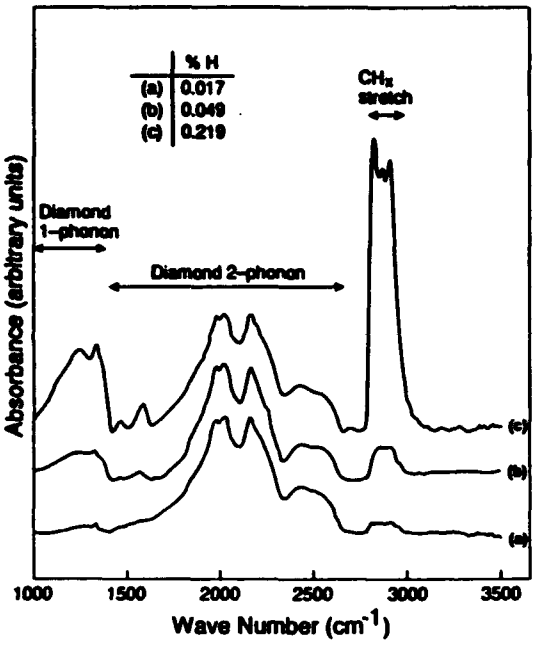

FIGURE 11. Absorption Spectra of Raytheon Hot-Filament CVD Diamond With H Content Varying From 0.017 to 0.219 Atom Percent (measured by solid-state ^1H nuclear magnetic resonance spectroscopy (Reference 8). Note the strong correlation between C-H stretching absorption and 1-phonon absorption.

Figure 13 shows details of the C-H stretching region of representative CVD diamond samples. As labelled at the top of the figure, the two C-H stretching frequencies of CH_2 groups in alkanes are found at 2925 ±10 and 2855 ±10 cm^{-1}. The two C-H stretching frequencies of CH_3 groups in alkanes are found at 2960 ±10 and 2870 ±10 cm^{-1}. The spectrum of paraffin wax in the lower part of Figure 13 is dominated by CH_2 groups, with smaller peaks from CH_3. The similarity of the C-H stretching region of CVD diamond to that of paraffin wax suggests that most of the hydrogen in diamond exists as CH_2 groups. In microwave plasma CVD diamond at the top of Figure 13, peaks corresponding to both CH_2 and CH_3 are observed. There is also a prominent unassigned peak at 2817 cm^{-1}, which we suggest may be due to hydrogen-capped diamond surfaces, such as the (100) surface that requires one hydrogen per carbon atom to complete the sp^3 tetrahedral bonding at the surface of the crystal.

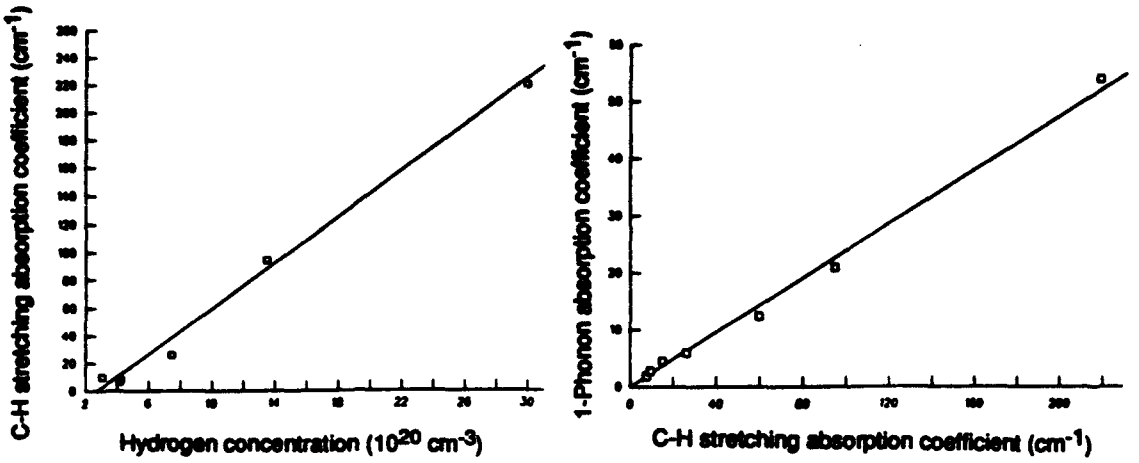

FIGURE 12. *Left:* Correlation Between C-H Infrared Absorption Near 3.5 μm and Hydrogen Content Measured by Nuclear Resonance Reaction Analysis in Texas Instruments dc Torch CVD Diamond. *Right:* Correlation between C-H absorption near 3.5 μm and broad absorption near 8 μm in the 1-phonon region (Reference 9).

^{1}H-nuclear magnetic resonance (NMR) spectroscopy of Raytheon hot-filament diamond shows a broad (50 to 70 kilohertz (kHz) wide) Gaussian signal indicative of highly segregated hydrogen atoms, probably at grain boundaries (Reference 8). Hydrogen is not randomly dispersed throughout the diamond. The majority of the hydrogen is rigidly held, while a fraction undergoes motional narrowing at room temperature. One interpretation is that most of the hydrogen is rigidly held as CH_2, and a small fraction is in CH_3 groups that are free to rotate.

From the transmission spectrum of paraffin in Figure 13, Norton estimated the absorption cross section for H in paraffin to be $\sigma = 2.6 \times 10^{-19}$ cm^2, for the 2920 cm^{-1} band. The cross section is defined by the equation

$$\text{Absorption coefficient (cm}^{-1}) = \alpha = \sigma N \qquad (4)$$

where N is the number density (atoms/cm^3) of hydrogen atoms. (The absorption cross section estimated from Figure 12 for the 2834 cm^{-1} band of diamond is 7×10^{-20} cm^2.) Norton used the cross section to estimate that the excellent quality diamond in Figure 14 contains 16 H atoms per million C atoms. In another experiment, Norton measured the hydrogen content of two different diamond samples by infrared absorption and by ^{1}H NMR. Infrared measurements gave H contents of 340 and 80 parts per million (ppm), while NMR gave values of 230 and 90 ppm for the same samples. This experiment confirms the validity of the infrared method for measuring hydrogen.

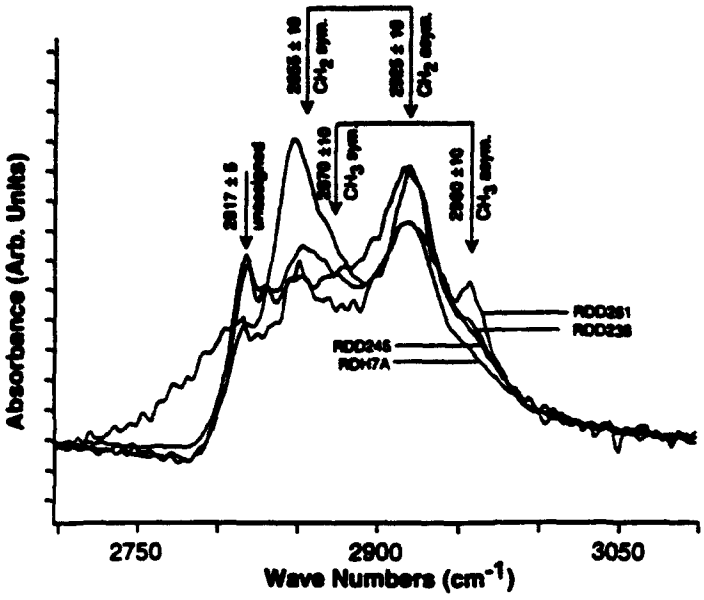

FIGURE 13. *Upper Spectrum* Shows C-H Stretching Region of Four Different Microwave Plasma CVD Diamond Samples From Raytheon. *Center spectrum* shows typical C-H stretching region of dc torch CVD diamond from Texas Instruments. *Lower spectrum* compares paraffin wax to Norton CVD diamond.

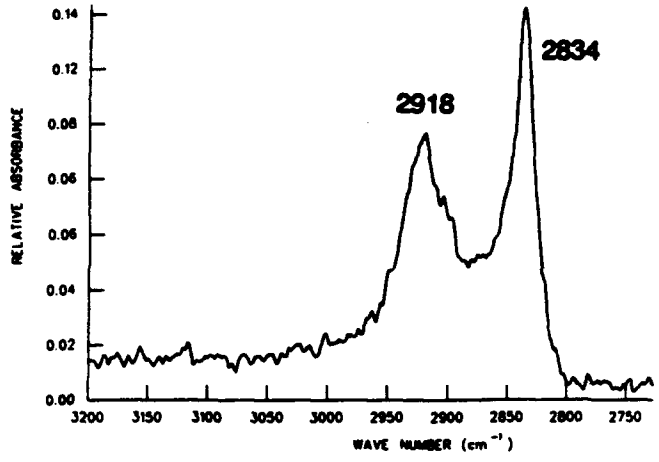

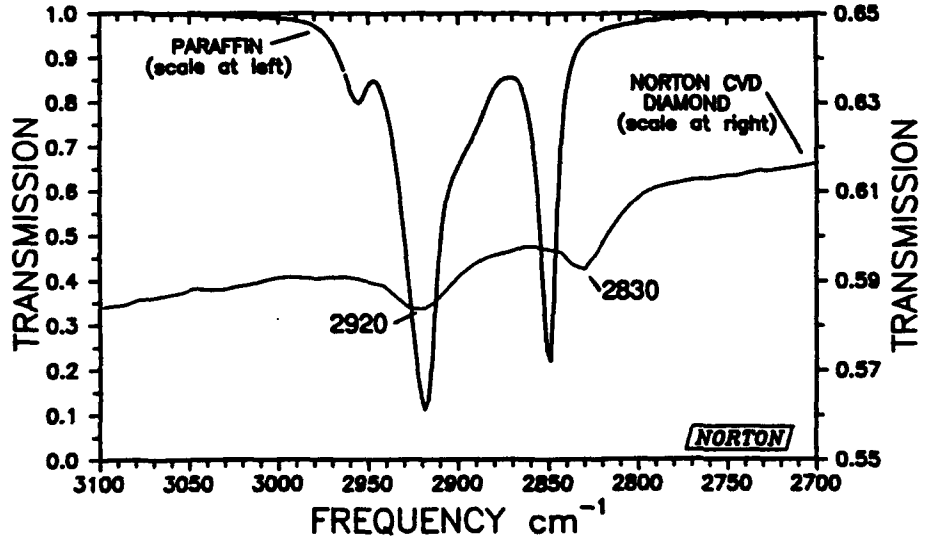

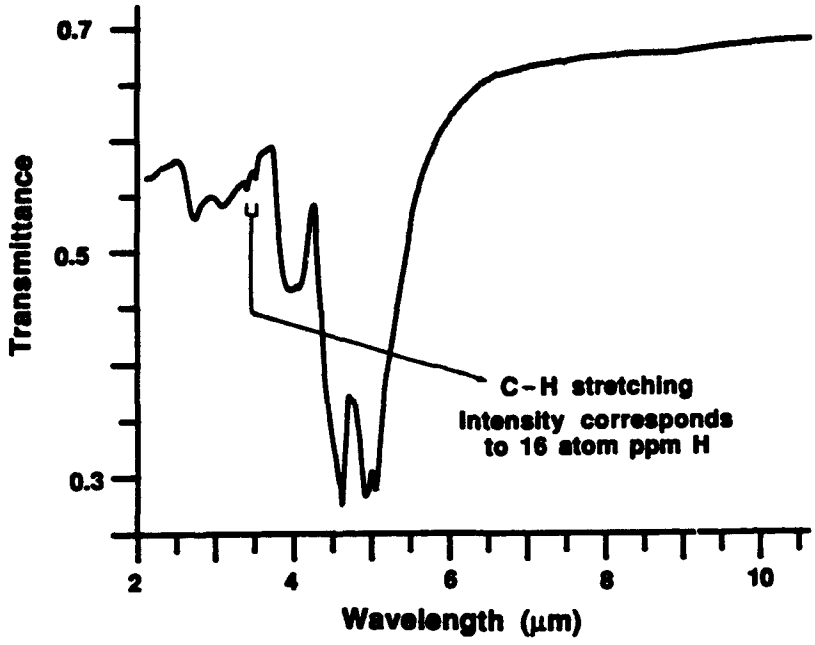

FIGURE 14. Transmission Spectrum of Norton Sample 30 With a Thickness of 0.638 mm From Growth Run TD1068, With C-H Stretching Absorption Intensity Corresponding to 16 H Atoms per Million C Atoms.

X-RAY AND MICROSCOPIC EXAMINATION OF DIAMOND SAMPLES

Numerous samples of polished, polycrystalline CVD diamond were received from Raytheon, Texas Instruments, and Norton in 1993. Figure 15 shows X-ray powder diffraction patterns from two specimens. The intensity pattern in the lower trace is similar to randomly oriented diamond powder, while the upper trace has a strong (220) reflection, indicating strong preferential (110) crystal orientation. In general, Texas Instruments' samples had orientations ranging from random to strong (110). Sometimes, two disks cut from different sections of the same growth run had these two different orientations, attesting to significant nonuniformity in deposition conditions. Norton samples were uniformly strongly (110) oriented. A single Raytheon disk (D382-02) that was examined had nearly random orientation.

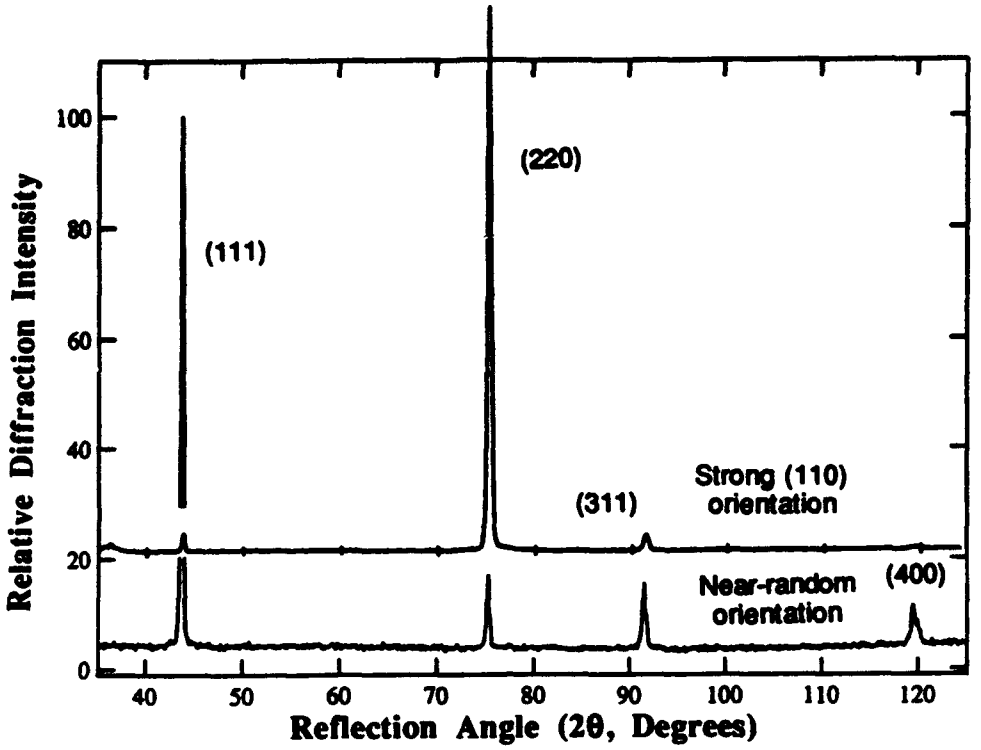

FIGURE 15. X-Ray Powder Diffraction Patterns of Texas Instruments CVD Diamond. Randomly oriented crystallites would have the following intensity pattern:

Angle (2θ)	d Spacing (Å)	Relative intensity	Miller indices
43°	2.060	100	(111)
75°	1.261	27	(220)
91°	1.075	16	(311)
119°	0.892	7	(400)
141°	0.818	15	(331)

Figures 16 and 17 contrast the fine (~10 μm) and coarse (~100 to 300 μm) grains on the substrate and growth surfaces of Norton diamond, in accord with the conical, columnar growth shown in Figure 6. Figure 18 shows a grain on a polished surface, with what appear to be fracture lines radiating into the grain from the boundaries. This could be a result of large stresses during growth, leading to fracture and stress relief. Figure 19 shows a section of what appears to be a fracture or void or nondiamond deposit running along (at grain boundaries?) for hundreds of micrometers, buried 570 μm beneath the surface of a sample that was almost a millimeter thick. A heavily twinned region of polished surface is seen in Figure 20. Figure 21 shows what appears to be a grain boundary going through a twin. It appears that there is epitaxial crystal growth across this grain boundary. None of the features in Figures 21-26 were unusual in the CVD diamond seen in this program.

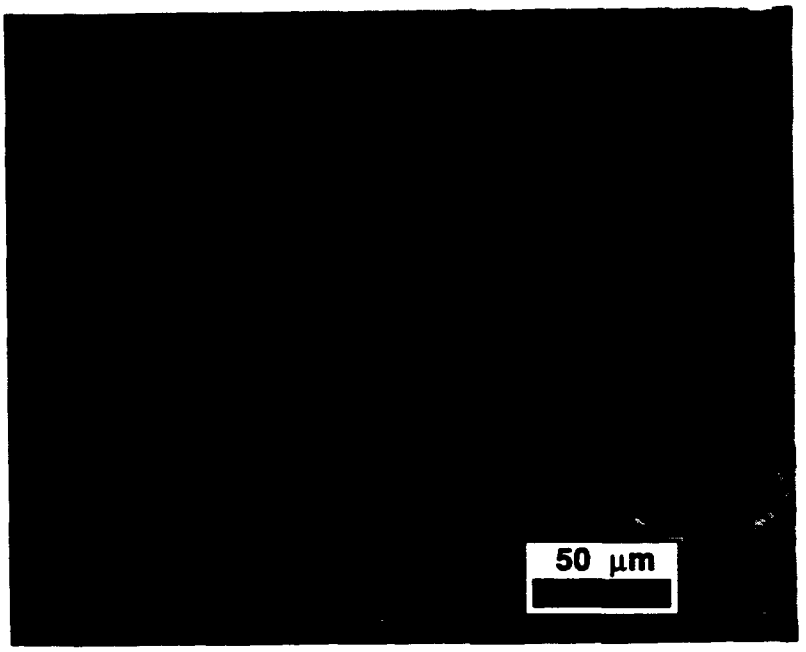

FIGURE 16. Fine Grain Structure of Substrate Surface of Polished Norton Diamond Specimen 12 (360×, transmitted light).

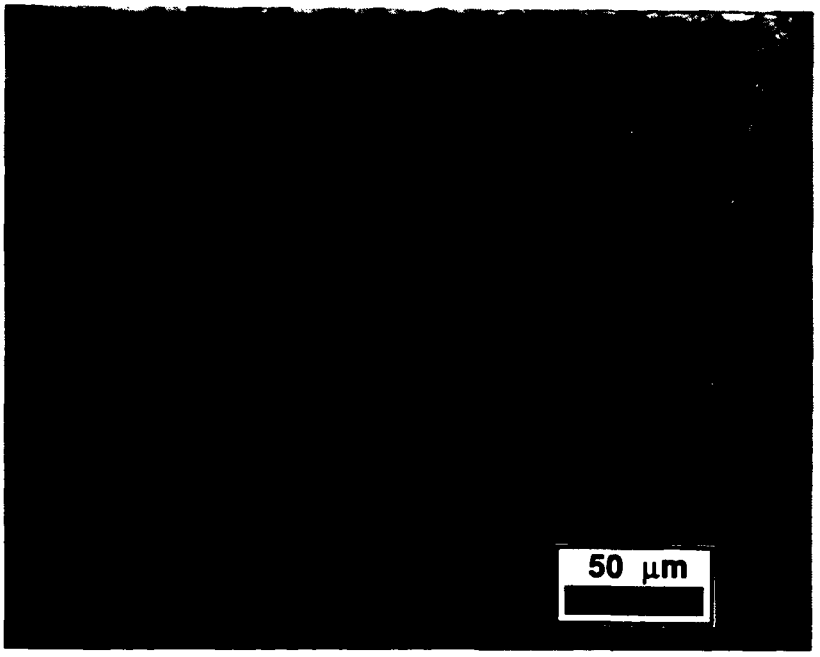

FIGURE 17. Coarse Grain Structure of Growth Surface of Polished Norton Diamond Specimen 12 (360×, transmitted light).

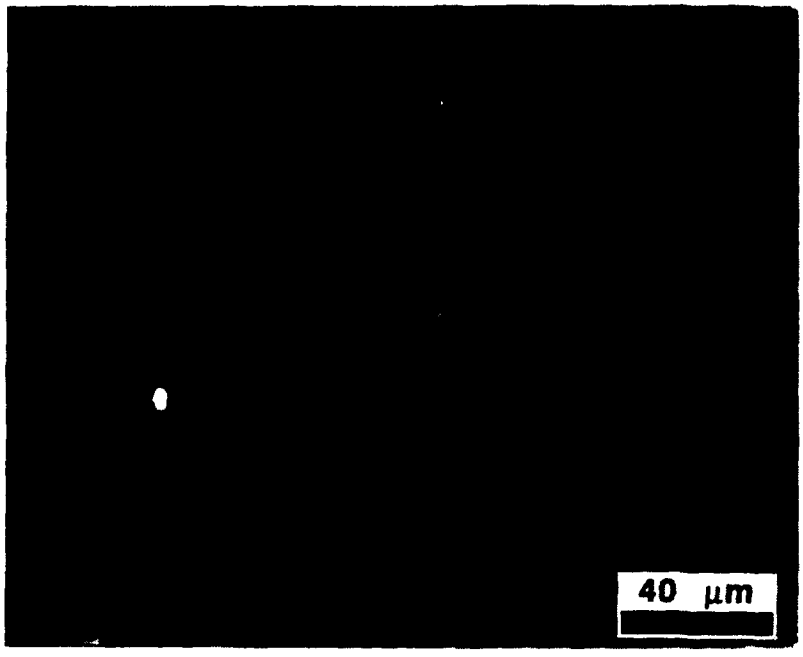

FIGURE 18. Surface of Polished Norton Diamond Specimen 5, With Fractures Apparently Running Into the Grain From the Edges (500×, transmitted light).

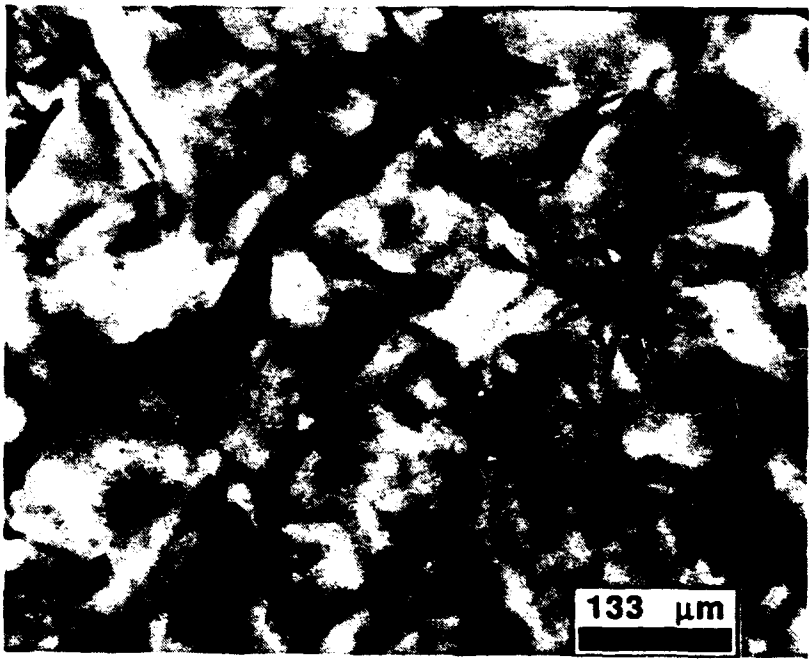

FIGURE 19. Long Defect 570 µm Beneath the Surface Appears to Run Along Grain Boundaries of Polished Raytheon Diamond Specimen H155-14 (150×, transmitted light).

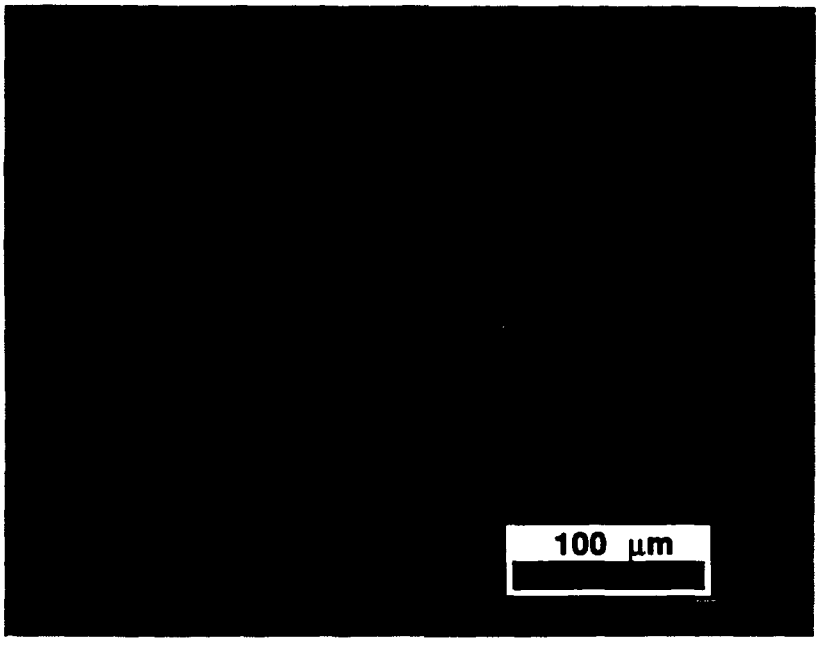

FIGURE 20. Crystal Twins on Polished Growth Surface of Norton Diamond Specimen 7 (250×, transmitted light).

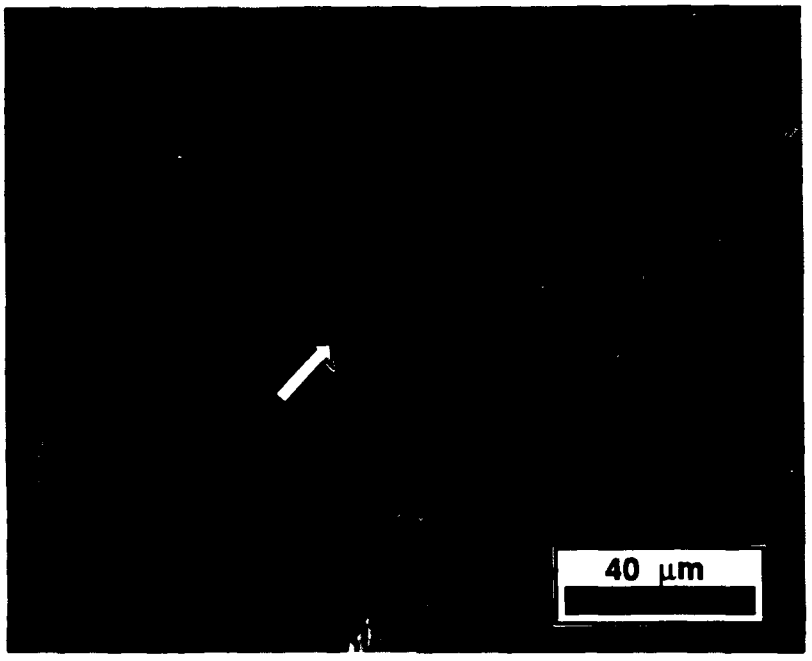

FIGURE 21. Grain Boundary (crooked line) Appears to Cross a Twin Boundary (straight line) on the Growth Surface of Polished Norton Diamond Specimen 23 (625×, transmitted light).

OPTICAL CHARACTERISTICS

BACKGROUND

If the radiant power entering a material is designated P_0, and radiant power P emerges after traversing a thickness t, the transmittance is P/P_0. Transmittance is related logarithmically to thickness:

$$P/P_0 = e^{-\alpha t} \tag{5}$$

where α is the absorption coefficient, with units of cm^{-1}. If the material reflects a fraction of incident radiation, R, at each surface, then the transmittance is

$$P/P_0 = \frac{(1 - R)^2 e^{-\alpha t}}{1 - R^2 e^{-2\alpha t}} \tag{6}$$

where $R = (n-1)^2/(n+1)^2$, and n is the refractive index. This equation applies to perpendicular incidence only.

Emissivity is defined as

$$\text{Emissivity} = \varepsilon = \frac{\text{radiant power emitted by material}}{\text{radiant power emitted by blackbody}} \tag{7}$$

and is related to the absorption coefficient by the equation

$$\varepsilon = \frac{(1 - R)(1 - e^{-\alpha t})}{1 - Re^{-\alpha t}} \tag{8}$$

for emission normal to the surface. For nearly transparent materials (with low small absorption coefficients), the expression for emissivity simplifies to

$$\varepsilon \approx \alpha t \quad (\text{for } \alpha t << 1) \tag{9}$$

LONG-WAVE INFRARED ABSORPTION

The best optical quality CVD diamond made at Raytheon, Norton, and Texas Instruments has adequate long-wave (8 to 14 μm) infrared optical properties for windows operating at 500°C. Transmission of the highest quality CVD diamond is similar to that of natural Type IIa diamond, which is the purest natural diamond (References 10 through 12). Figure 22 shows the behavior of the infrared spectrum of diamond up to 515°C (788 K) and Figure 23 shows that the absorption coefficient in the 2-phonon region increases by 50% from 25 to 700°C. In general, there is little temperature dependence in the 1-phonon region, some change in the 2-phonon region, and more in the 3-phonon region. Theoretically, the absorption coefficient should be proportional to temperature (T) in the

2-phonon region and proportional to T^2 in the 3-phonon region at sufficiently high temperature. The observed increase in absorption of diamond is less than the high-temperature limit (Reference 12).

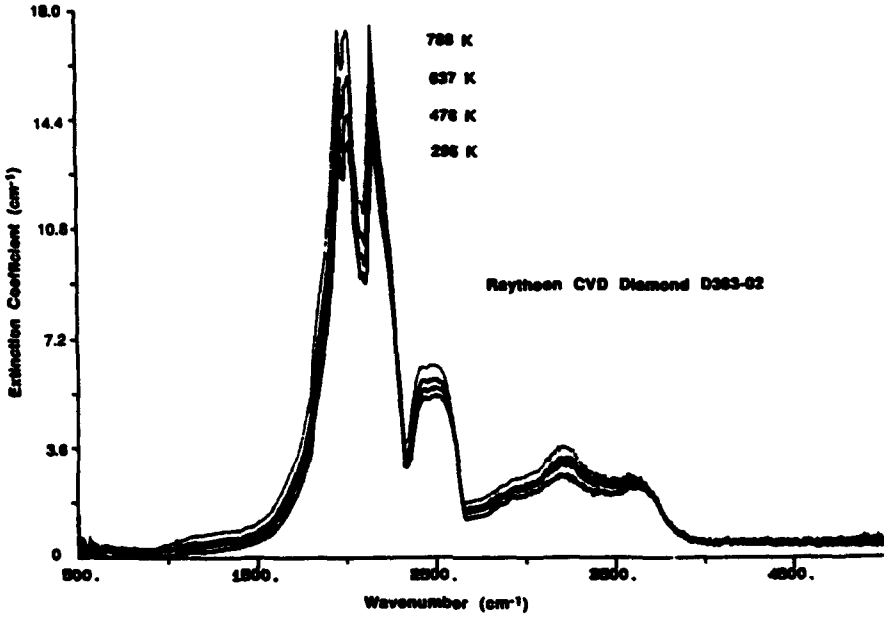

FIGURE 22. Infrared Absorption of Raytheon CVD Diamond Specimen D383-02 (0.75 mm thick) (Courtesy M. E. Thomas, Applied Physics Laboratory, Laurel, Md. (Reference 11).) Spectra in this and the next figure were recorded on different spectrometers. The apparently larger temperature variation of specimen D383-02 in the 500-1500 cm^{-1} region may not be correct.

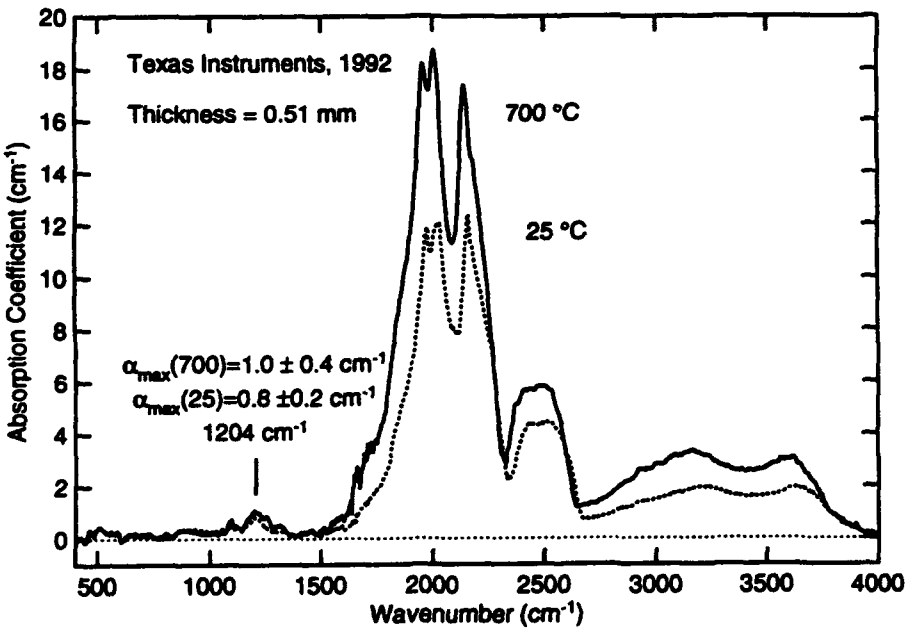

FIGURE 23. Temperature Dependence of Infrared Absorption of 0.51-mm-Thick Texas Instruments CVD Diamond.

Figure 24 compares the very weak absorption of Type IIa diamond in the 1-phonon region to that of two specimens of excellent-quality CVD diamond. Natural diamond has weak absorption maxima at 1050, 890, 810, and 740 cm^{-1} that are just barely evident in Figure 24 (Reference 12). These are superimposed on a low-energy tail from the 2-phonon region that is labeled "theoretical model" in Figure 24 and given by the equation (Reference 12)

$$\text{2-phonon tail in 1-phonon region:} \qquad \alpha\ (cm^{-1}) = \frac{146\ \omega^5}{\omega_{max}{}^6}\ (\text{for } \omega < \omega_{max}) \tag{10}$$

where α is the absorption coefficient, ω is wavenumber (cm^{-1}), and $\omega_{max} = 1143\ cm^{-1}$. This is an acoustic contribution to absorbance in the 1-phonon region from 2-phonon modes. The constant 146 cm^{-2} was obtained by fitting the tail to points measured by laser calorimetry for Type IIa diamond (Table 2).

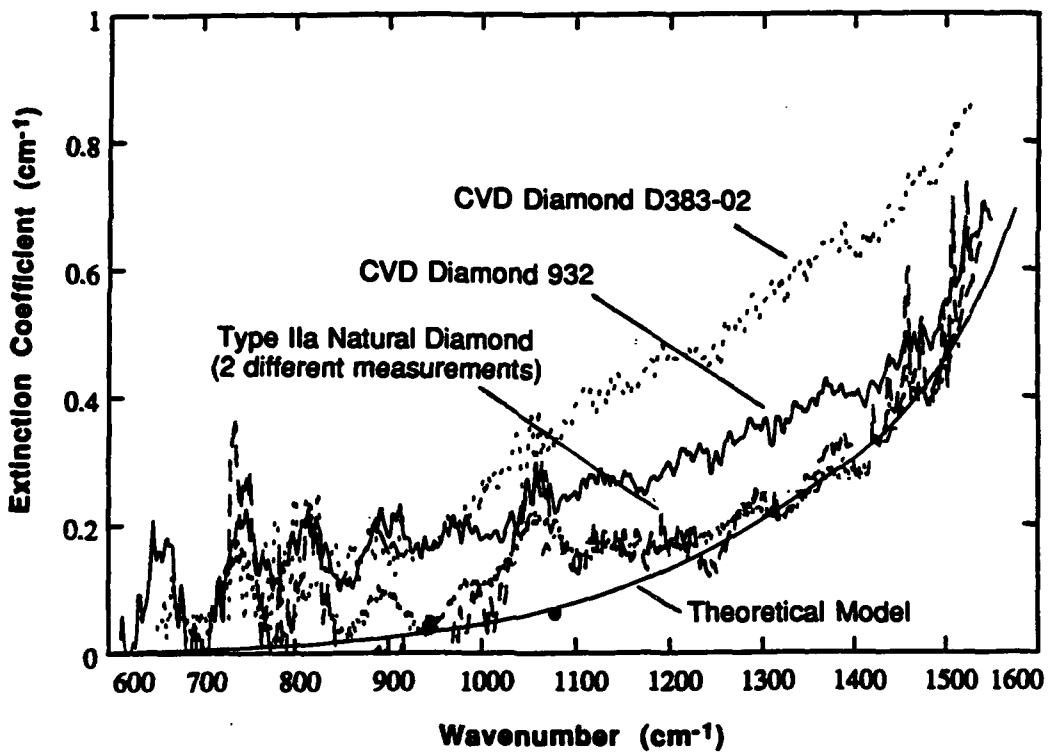

FIGURE 24. Infrared Absorption of Diamond. The extinction coefficient includes the combined effects of scatter and absorption. Sample D383-02 is the highest quality CVD diamond received in the Navy program. Sample 932 is the highest quality CVD diamond that has been examined at the Applied Physics Laboratory. Points at 944 and 1079 cm^{-1} are laser calorimetry measurements on Type IIa diamond (Table 2). The smooth curve is from Equation 10 (Courtesy M. E. Thomas, Applied Physics Laboratory (Reference 11).

TABLE 2. Laser Calorimetric Measurement of Type IIa Diamond Absorption Coefficient.[a]

Wavenumber, cm^{-1}	Absorption coefficient, cm^{-1}	Reference
944 (10.6 μm)	0.033, 0.042	13
944 (10.6 μm)	0.047	Raytheon
1079 (9.27 μm)	0.062	Raytheon

[a] An additional estimate of the absorption coefficient of Type IIa diamond at 944 cm^{-1} is $\alpha = 0.024\ cm^{-1}$ from transmission data in Figure 2 of Reference 14).

Absorption coefficients for natural diamond may be compared to those of several good quality CVD diamond samples. The absorption coefficient of Raytheon diamond in Table 3 is approximately 0.1-0.2 cm^{-1}, and doubles upon heating to ~500°C. The absorption coefficient of Norton diamond in Table 4 is approximately twice as high as that of the best Raytheon sample and also doubles upon heating to ~500°C. For comparison, transmission spectra of natural Type IIa diamond (sample 806) at the Applied Physics Laboratory show that the absorption coefficient at 10 μm also doubles, from 0.1 cm^{-1} at 20°C to 0.2 cm^{-1} at 770°C. Absorption coefficients of five Texas Instruments diamond samples in Table 5 are 0.15 to 0.35 cm^{-1} at 10.6 μm at 25°C.

TABLE 3. Infrared Absorption Coefficient of Raytheon CVD Diamond D383-02 (0.75 mm thick).

Absorption coefficient, cm^{-1}, at 10.6 μm		
Value	Measurement made at	Method
0.07	Raytheon	laser calorimetry
0.11 ±0.03	Texas Instruments	laser calorimetry
0.23 ±0.04	China Lake	laser calorimetry
0.15	Texas Instruments	transmission spectrum
0.12	Rockwell Science Center	transmission spectrum
0.16	Applied Physics Lab	transmission spectrum
Average absorption coefficient, cm^{-1}, from 8-14 μm based on transmission spectrum		
Value	Measurement made at	Temperature, °C
0.10 ±0.05	Texas Instruments	20
0.18 ±0.05	Texas Instruments	470
0.30	Rockwell Science Center	20
0.62	Rockwell Science Center	475

TABLE 4. Infrared Absorption Coefficient of Norton CVD Diamond Sample 24 (0.54 mm thick).

Absorption coefficient, cm^{-1}, at 10.6 μm		
Value	Measurement made at	Method
0.30 ± 0.10	Texas Instruments	laser calorimetry
0.53 (+0.03 -0.15)	China Lake	calorimetry on Sample 23 (from same growth run as #24)
0.20	Texas Instruments	transmission spectrum
0.36	Rockwell Science Center	transmission (@ 10.0 μm)
0.16	Applied Physics Lab	transmission spectrum
Average absorption coefficient, cm^{-1}, based on transmission spectrum		
Value	Measurement made at	Temperature, °C
0.15 ±0.10 @ 8-14 μm	Texas Instruments	20
0.25 ±0.10 @ 8-14 μm	Texas Instruments	477
0.37 @ 8-12 μm	Rockwell Science Center	20
0.64 @ 8-12 μm	Rockwell Science Center	475

TABLE 5. Infrared Absorption Coefficient of Texas Instruments CVD Diamond NW3-74B (0.36 mm thick).

Average absorption coefficient, cm^{-1}, based on transmission spectrum		
Value	Measurement made at	Temperature, °C
0.20 @ 8-14 μm	Texas Instruments	25
0.30 @ 8-14 μm	Texas Instruments	650
Absorption coefficient (cm^{-1}) of 4 different samples at 10.6 μm at 25°C		
Value	Measurement made at	Method
0.15	Texas Instruments	laser calorimetry
0.20	Texas Instruments	laser calorimetry
0.25	Texas Instruments	laser calorimetry
0.35	Texas Instruments	laser calorimetry

Extrapolations of laser calorimetric absorption coefficients to zero thickness for Type IIa and CVD diamond in Figure 25 indicate that surface absorption is negligible compared to bulk absorption. The transmission spectrum of a diamond film in Figure 26 demonstrates that diamond has no far infrared absorption at wavenumbers down to 18 cm^{-1} (556 μm).

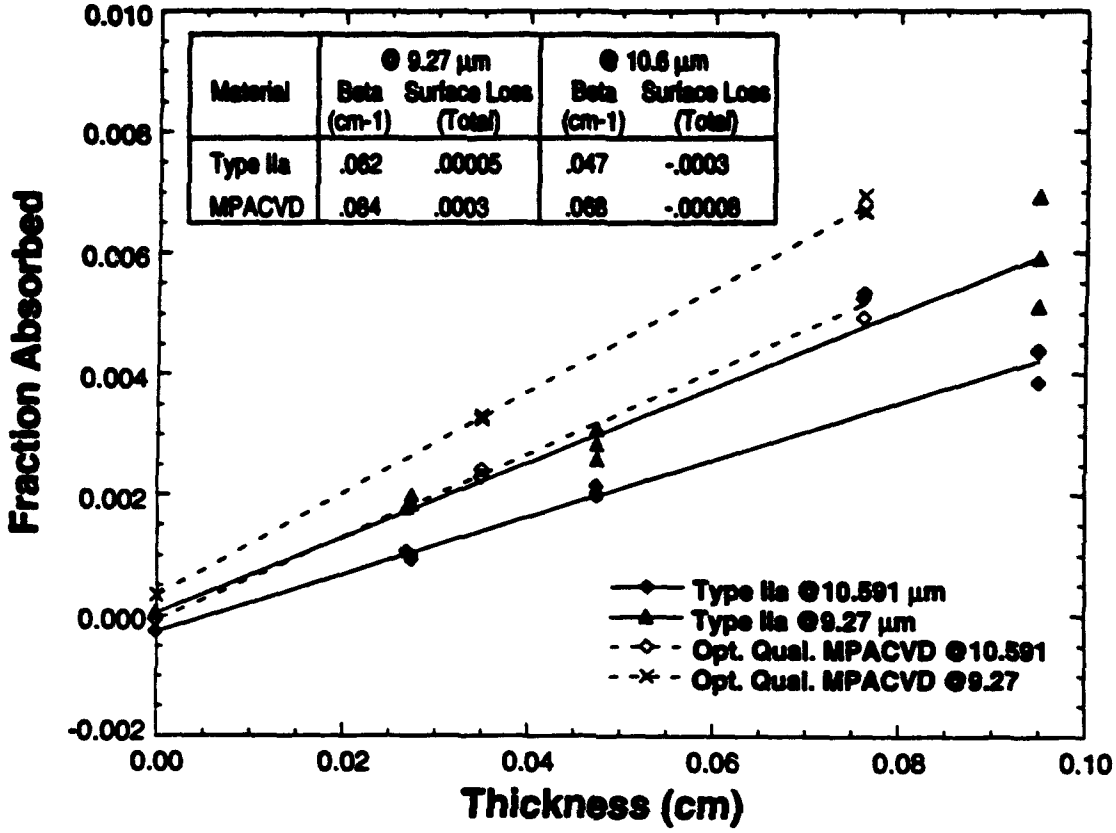

FIGURE 25. Absorption Coefficient of Type IIa and Microwave-Plasma-Assisted Chemical-Vapor-Deposited Diamond (MPACVD) as a Function of Thickness, Measured by Laser Calorimetry at Raytheon. Since all lines extrapolate close to zero absorption at zero thickness, the absorption arises predominantly from the bulk diamond, not the polished surfaces.

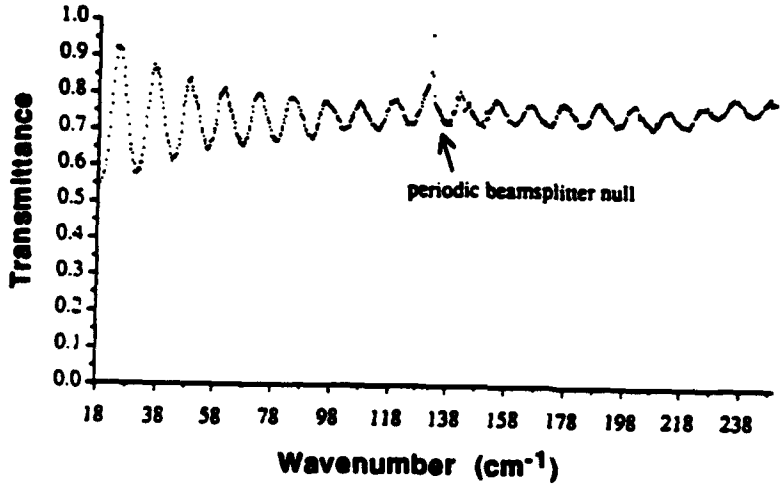

FIGURE 26. Very Long-Wave Infrared Transmission of Raytheon Hot-Filament Diamond HFB21, Recorded at the University of Lowell (Mass.). Assuming a refractive index of 2.38, the interference fringe pattern indicates that the thickness of the sample is 184 µm.

LONG-WAVE INFRARED EMISSION

Emission from samples heated in a furnace was measured at Rockwell Science Center using an 8-to-12 μm bandpass filter. Graphite was used as a standard, with an assumed emissivity of 0.96. High-quality specimens from Raytheon and Norton had emissivities of ~0.02 at 300°C and 0.03 near 500°C. Spectrally resolved emissivity of high quality CVD diamond from a different source is shown in Figure 27.

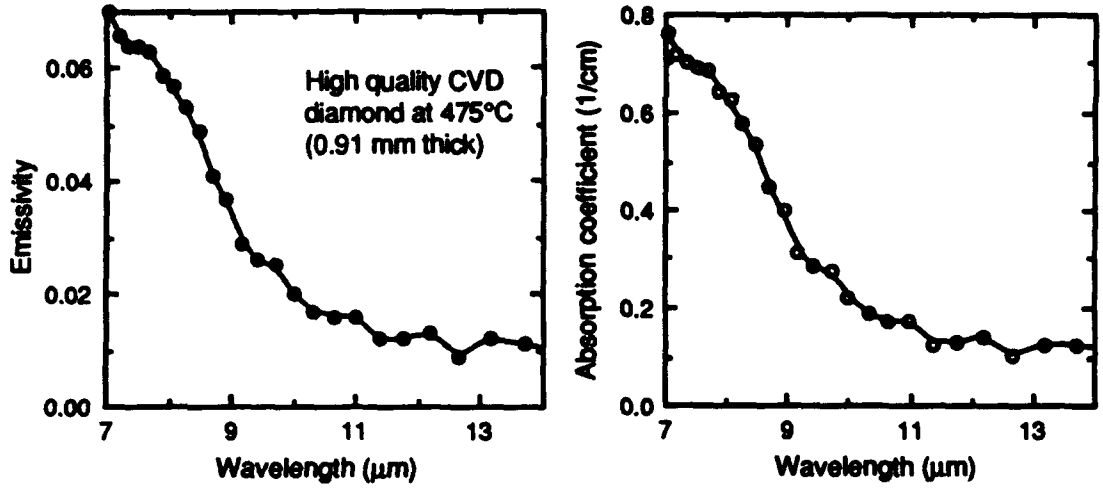

FIGURE 27. Emissivity of High Quality CVD Diamond at 475°C (thickness = 0.91 mm). The absorption coefficient at the right is derived from the emissivity at the left.

OPTICAL SCATTER

The best quality polycrystalline CVD diamond has ~100 times as much scatter as single crystal Type IIa diamond at 10.6 μm and ~20 times as much scatter at 0.63 μm (Table 6). However, the long-wave infrared scatter of high quality CVD diamond is below 1% and acceptable for most applications. There is no change in the scatter of Type IIa or CVD diamond upon going from 20 to 500°C (Reference 10). Table 6 compares optical scatter for natural diamond to scatter from the highest quality CVD diamond. Table 7 shows scatter for numerous CVD specimens. Forward scatter is greater than back scatter in CVD diamond at wavelengths of 0.63 and 3.39 μm, while back scatter is greater than forward scatter at 10.6 μm.

TABLE 6. Comparison of Integrated Forward Scatter of Type IIa Diamond and the Highest Quality CVD Diamond.

Sample	Thickness	Scatter, 0.63 μm	Scatter, 10.6 μm
Type IIa (806)[a]	0.50 mm	0.2%[b]	0.004%[c]
CVD Raytheon D383-02	0.75 mm	4%[d]	0.4%[d]

[a] Reference 10.
[b] Bidirectional transmittance distribution function (BTDF) (Reference 15) measurement integrated from 0.3 to 45°.
[c] BTDF measurement integrated from 1.1 to 45°.
[d] Total integrated scatter (Reference 16) from 2.5 to 70° measured with integrating sphere.

TABLE 7. Total Integrated Scatter (Reference 16) of CVD Diamond Specimens.[a]

	Forward scatter, %/Back scatter, %		
Source	Wavelength, 0.63 μm	Wavelength, 3.39 μm	Wavelength, 10.6 μm
Type IIa			
806[b]	...	...	0.004/0.012 (BTDF 2.3-80° integration) (BRDF 5.5-80° integration)[c]
Raytheon			
H157-01	4.5/2.2	0.84/0.43	0.13/0.45
D362-01	2.3/1.3	0.61/0.20	0.9/0.20
H155-10	6.5/1.7	9.0/1.4	3.9/5.4
H155-16	9.2/3.6	4.6/1.5	1.5/3.1
D383-02	4.2/1.9	1.0/...	0.36/0.8 (0.22% forward scatter measured by BTDF method[d] for D383-02)
Texas Instruments			
NW2-78E	12/2.4	17/2.2	6.7/8.9
Norton			
1 (TD 994)	29/8.7	8.6/2.4	1.4/2.7
9 (TD 994)	28/7.4	8.7/1.8	1.7/2.9
13 (TD 1022)	19.4/7.3	5.8/2.1	1.3/2.3
23 (TD 1068)	23.6/7.8	4.5/1.3	0.6/1.0

[a] All samples except Type IIa were measured with integrating sphere from 2.5 to 70°.
[b] Reference 10.
[c] Bidirectional reflectance distribution function (BRDF).
[d] Reference 15.

The root-mean-square surface roughness of polished CVD diamond from Raytheon and Texas Instruments was ~10 nm, while diamond from Norton had a roughness near 40 nm. Using the expression total integrated scatter $\approx (4\pi\delta/\lambda)^2$, where δ is surface

roughness and λ is wavelength, the surface scatter contribution for Raytheon and Texas Instruments diamond is expected to be ~4% at visible wavelengths. This could account for most of the visible scatter in the highest quality samples.

Figure 28 shows the angular dependence of forward and back scatter of single crystal Type IIa diamond at a wavelength of 10.6 μm (measured by the BTDF and BRDF methods (Reference 15)). Figure 29 shows that the angular dependence of forward scatter of the highest optical quality polycrystalline CVD diamond is much broader than the scatter from single crystal Type IIa diamond. Figure 30 shows that visible (0.63 μm) and midwave infrared (3.39 μm) scatter from one high quality CVD diamond sample are similar, and substantially greater than long-wave infrared (10.6 μm) scatter.

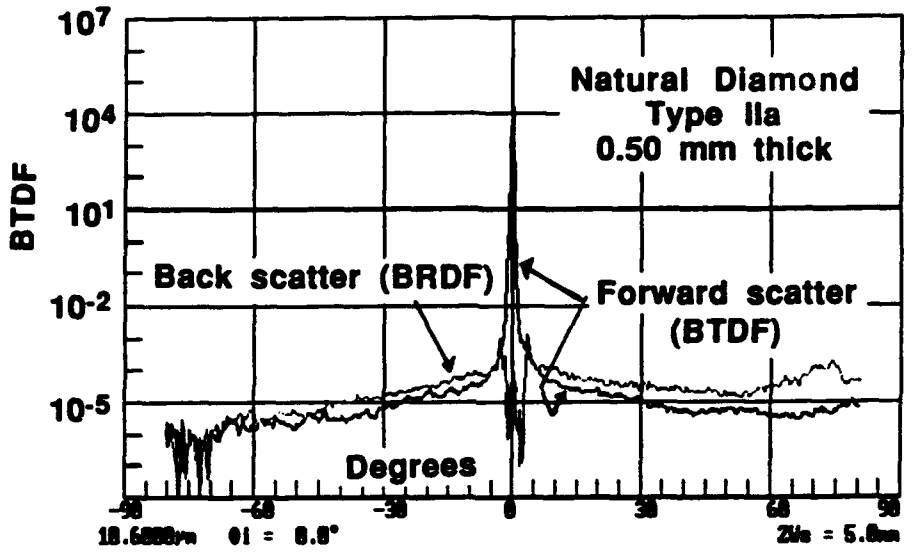

FIGURE 28. Forward and Back Scatter of Natural Type IIa Diamond at 10.6 μm (Reference 10).

The transmission spectrum of 100-μm-thick, polished CVD diamond recorded with a 40 × 40 μm aperture in Figure 31 shows that most of the optical scatter originates at the grain boundary, not the grain center. This is consistent with the notion that grain boundaries contain nondiamond (hydro)carbon.

REFRACTIVE INDEX AND MICROWAVE DIELECTRIC PROPERTIES

Literature values for the refractive index of Type IIa diamond are shown in Table 8. The best measurement of refractive index of CVD diamond that we are aware of comes from the strong interference pattern of Norton diamond disk 24 in Figure 32. The disk is thicker in the center (517 ±5 μm) than around the edges (511 ±5 μm). There are 10 fringes between 964.08 and 923.23 cm^{-1}. Using the center thickness, the refractive index is calculated to be 2.37 ±0.02. The edge thickness gives a refractive index of 2.40 ±0.02. Since the beam was directed at the center of the specimen, we consider these measurements to be consistent with the literature value of 2.38 near 10 μm. The temperature dependence

of the refractive index (n) of this specimen, based on the shift of interference fringes in the transmission spectrum measured at the Applied Physics Laboratory, is:

$$\frac{dn}{dT} = 13 \times 10^{-6}\ K^{-1} \text{ at } 10\ \mu m \text{ (average for T = 295 to T = 784 K)} \qquad (11)$$

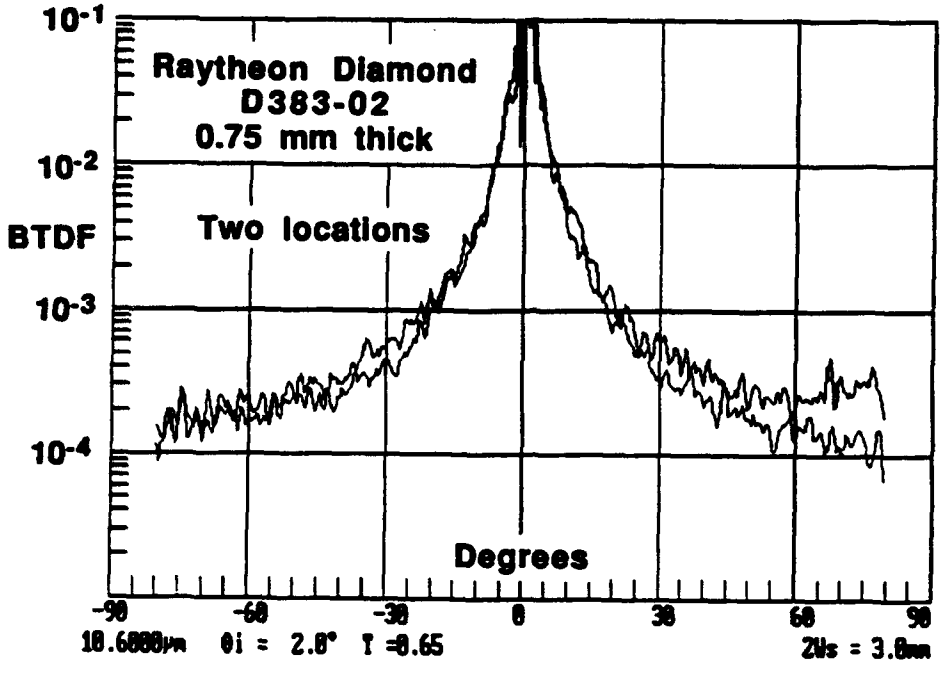

FIGURE 29. Forward Scatter of High Quality CVD Diamond at 10.6 μm.

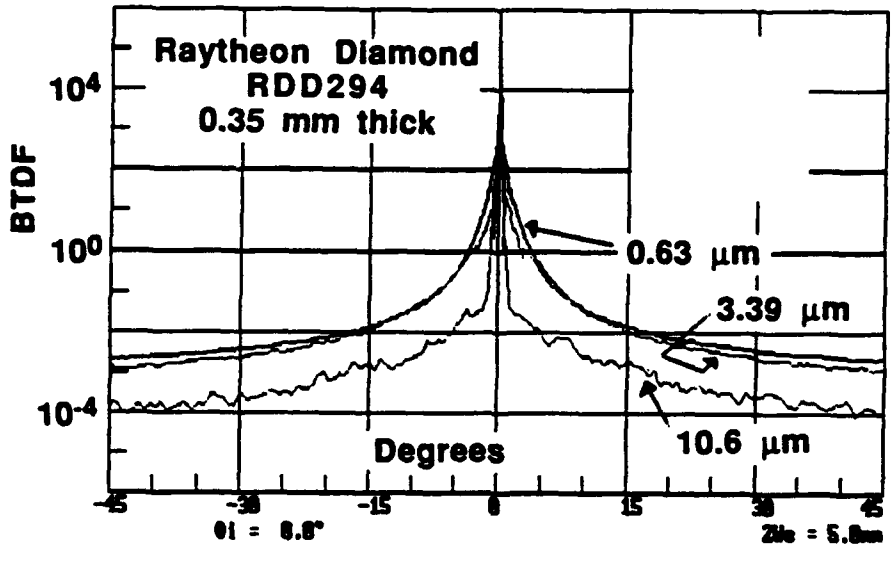

FIGURE 30. Forward Scatter of High Quality CVD Diamond at Different Wavelengths (Reference 10).

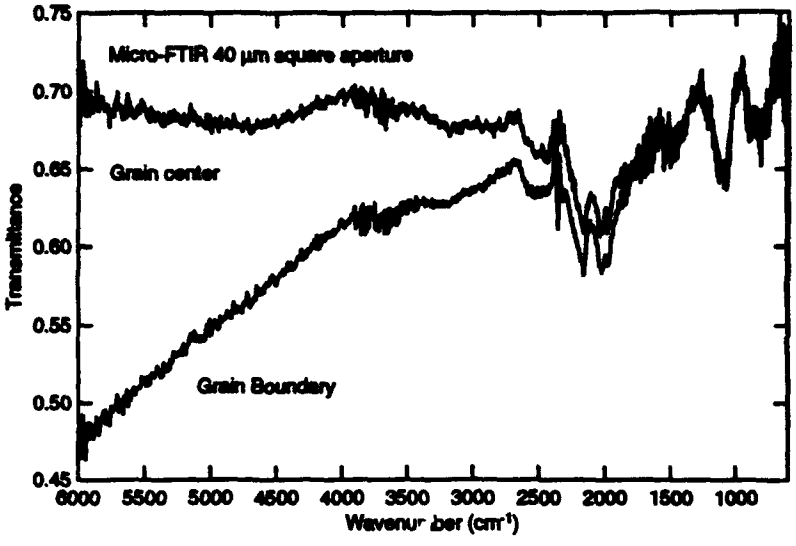

FIGURE 31. Infrared Transmission Spectrum of 100-µm-Thick, Polished CVD Diamond Recorded at Texas Instruments With a 40 µm x 40 µm Aperture. Optical scatter is enhanced at the grain boundary.

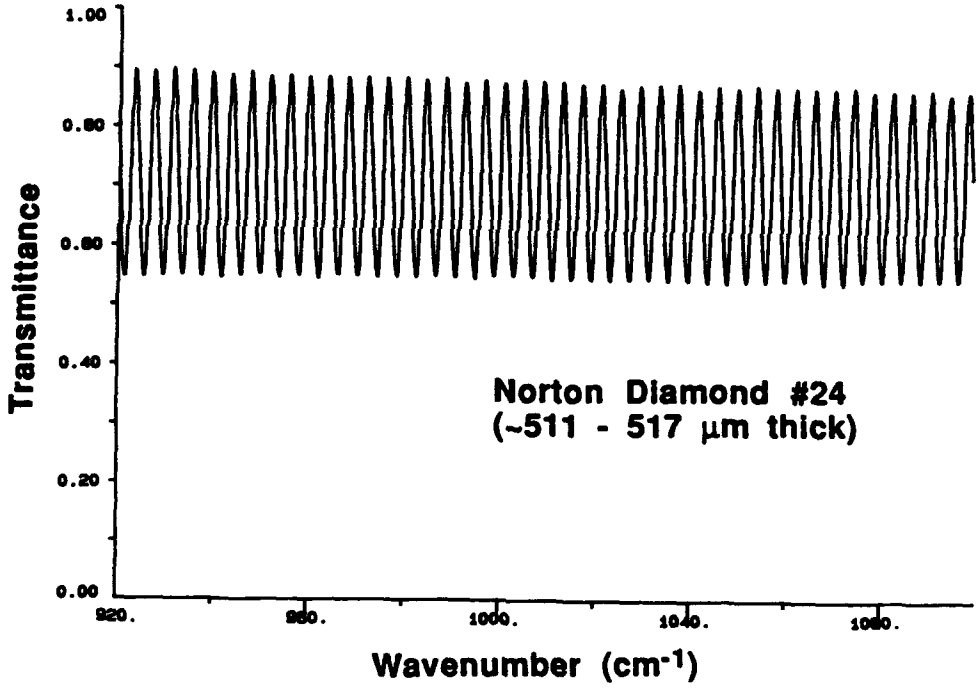

FIGURE 32. Strong Interference Fringes in the Transmission Spectrum of Norton Diamond Specimen 24 are Consistent With the Literature Value of the Refractive Index of Type IIa Diamond of 2.38 Near 10 µm (Spectrum courtesy of M. Thomas, Applied Physics Laboratory).

TABLE 8. Refractive Index of Type IIa Diamond.[a,b]

Wavelength, μm	Refractive index	Wavelength, μm	Refractive index	Wavelength, μm	Refractive index
0.25	2.638	0.70	2.404	6.00	2.378
0.30	2.544	2.50	2.380	8.00	2.377
0.40	2.463	3.00	2.380	10.00	2.376
0.50	2.430	4.00	2.379	14.00	2.375
0.60	2.413	5.00	2.378	20.00	2.374

[a] Reference 17.

[b] The dependence of refractive index on temperature is $(1/n)(dn/dT) = 4.04 \times 10^{-6}\ K^{-1}$ and the dependence on pressure is $(1/n)(dn/dP) = -0.36 \times 10^{-12}\ Pa^{-1}$ near 300 K (Reference 18). Temperature dependence was measured at frequencies below $\leq 10^4$ Hz, but should apply to the long-wave infrared region.

The low frequency ($\leq 10^4$ Hz) dielectric constant of Type IIa diamond is reported to be 5.70 (Reference 18). This value is expected to be independent of frequency throughout the microwave region. Numerous measurements of the dielectric constant of different samples of CVD diamond have given values near 5.7, with loss tangents as low as $\leq 2 \times 10^{-4}$. Early developmental samples of impure CVD diamond had a dielectric constant as low as 4.2 and loss tangents that were 2-3 orders of magnitude greater than those of very pure samples.

THE RAMAN SPECTRUM OF IMPERFECT DIAMOND DEPENDS ON EXCITATION WAVELENGTH

Type IIa diamond exhibits a single sharp Raman peak near 1333 cm^{-1} at 20°C. Under compression this peak shifts to higher frequency, so it may be used as a measure of stress in diamond (Reference 19). However, the effect of stress is anisotropic (producing differing shifts for the same pressure directed along different crystal axes), and the single peak splits into multiple components under anisotropic stress.

In general, the higher the quality of the diamond, the narrower is the 1333 cm^{-1} peak. Figure 33 shows that laser Raman excitation at 1.064 μm is much more sensitive to the quality of the diamond than is Raman excitation at 488 nm. (Qualitatively similar results have been reported before (Reference 20). In the upper part of the figure, spectra of two moderate-optical-quality samples have weak peaks at 1333 cm^{-1}, surrounded by strong, broad signals that presumably arise from nondiamond carbon. Only the very high quality specimen D362-01 gives a reasonably (but not completely) clean spectrum, with weak, broad signal between 1000 and 1600 cm^{-1}. In the lower spectrum, excitation of Specimen H155-16 at 488 nm gives a clean, sharp signal at 1333 cm^{-1}.

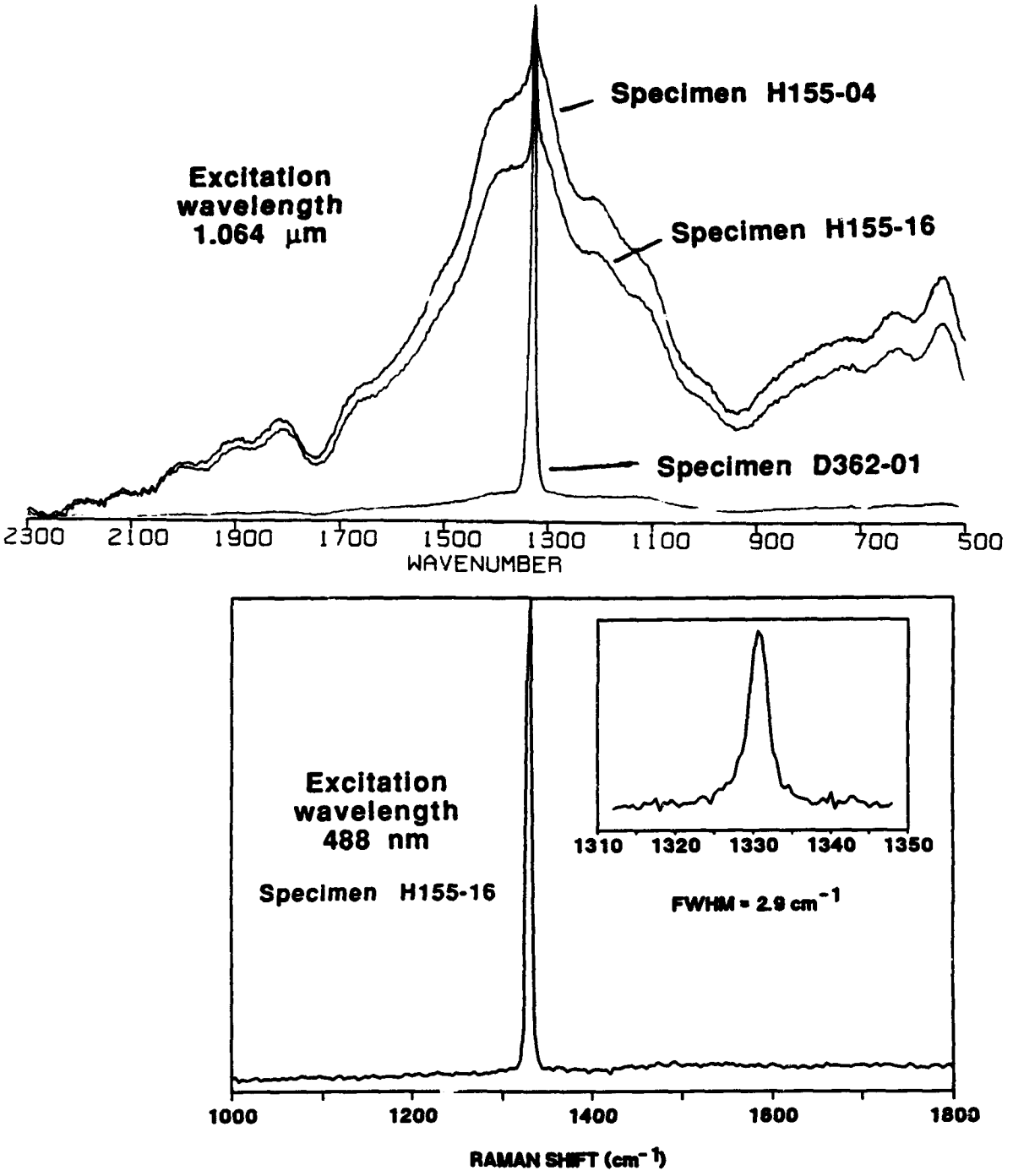

FIGURE 33. *Upper Figure* Shows Raman Spectra of Three Different Raytheon CVD Diamond Samples With Laser Excitation at 1.064 μm. Specimen D362-01 is colorless and transparent. Specimens H155-04 and H155-16 are light gray and transparent, but have a high density of dark spots. *Lower figure* shows Raman spectrum of specimen H155-16 with laser excitation at 488 nm. The inset shows that the width of the peak at half-height is 2.9 cm^{-1} (Data from M. Nadler and W. Weimer, Naval Air Warfare Center Weapons Division (NAWCWPNS), China Lake, Calif.).

Figure 34 shows that the linewidth of diamond excited at 488 nm is correlated with the linewidth of diamond excited at 1.064 μm. In a previous study (Reference 20), it was found that the linewidth of the 1333 cm^{-1} peak is greater with ultraviolet excitation (351 and 257 nm) than with visible excitation. Furthermore, with ultraviolet excitation, the spectrum is insensitive to nondiamond carbon and only exhibits the 1333 cm^{-1} peak. None of these effects are understood. A correlation between the linewidths of Raman and ^{13}C-NMR signals from diamond has also been reported (Reference 21). The better the quality of the diamond, the narrower is the NMR linewidth.

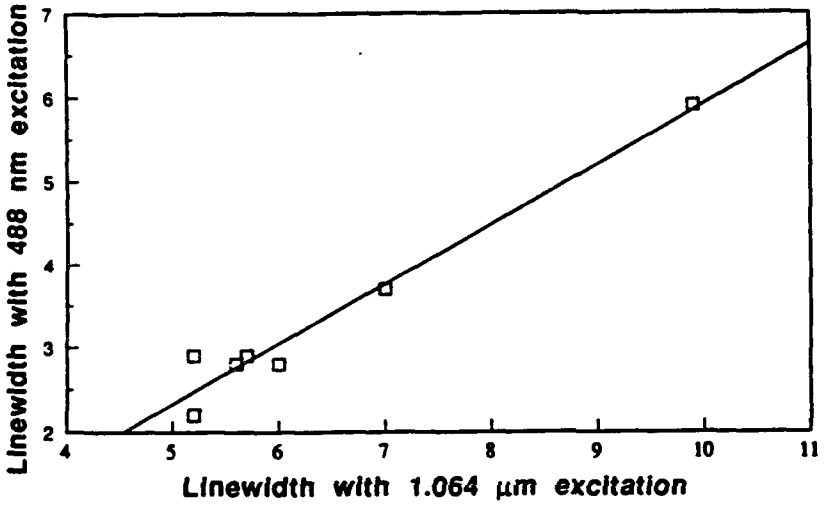

FIGURE 34. Linewidth of 1333 cm^{-1} Raman Peak of CVD Diamond Excited at 488 nm is Correlated With Linewidth Arising From Excitation at 1.064 μm (Data from M. Nadler and W. Weimer).

THERMAL EXPANSION AND THERMAL CONDUCTIVITY

The thermal expansion coefficient (α) of CVD diamond is nearly the same as that of natural diamond (Figure 35). The polynomial fit to the CVD expansion data is

$$\alpha = \frac{1}{L}\frac{dL}{dT} = 1.1277 + 6.5426 \times 10^{-3}\,T - 1.4382 \times 10^{-6}\,T^2 \qquad (12)$$

where L is the length of the sample, T is °C, and α is given in parts per million.

Thermal conductivity of CVD diamond was studied at Raytheon, with representative results in Figure 36. Figure 37 shows the thermal conductivity calculated for diamond with different grain sizes (Reference 22). At low temperature, phonon scattering at grain boundaries limits the conductivity of polycrystalline diamond. Above 500 K, there is little dependence on grain size, since phonon-phonon scattering occurs over distances smaller than the grain size. In fact, experimental measurements at low temperature indicate that the mean free path for phonons in polycrystalline diamond can be 4-10× greater than the grain size (Reference 23). Differing shapes of the experimental conductivity curves in Figure 36 are attributed to phonon scattering from defects in the hot-filament CVD diamond that are not present in the higher quality microwave plasma diamond (Reference 24).

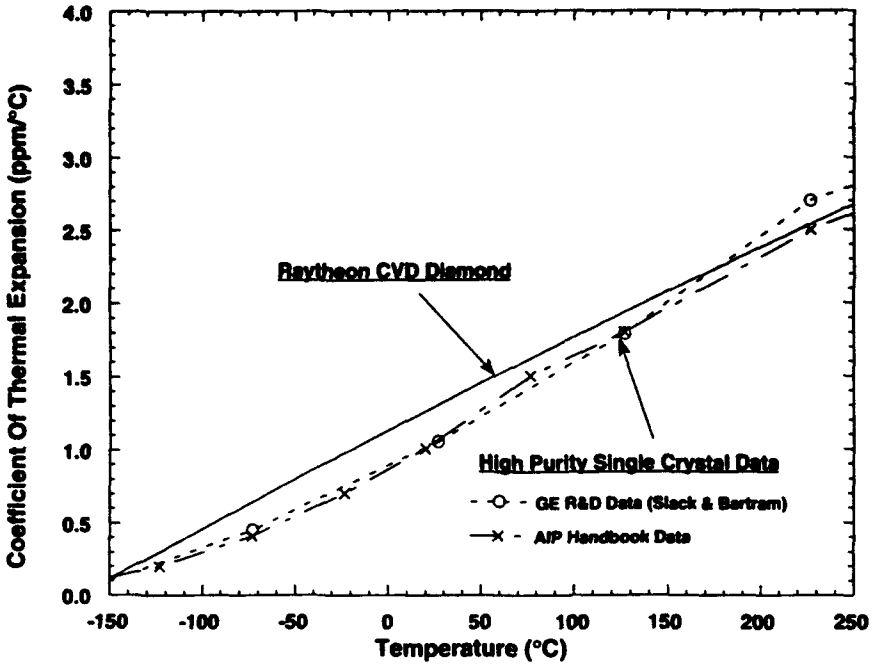

FIGURE 35. Thermal Expansion Coefficient of Single Crystal Diamond and Raytheon Specimen RDH31. Expansion of 25-mm-long bar of CVD diamond was measured with a silica reference. Recent measurements show that the thermal expansion of CVD and natural diamond are the same over the range 50-1100 K (Reference 25).

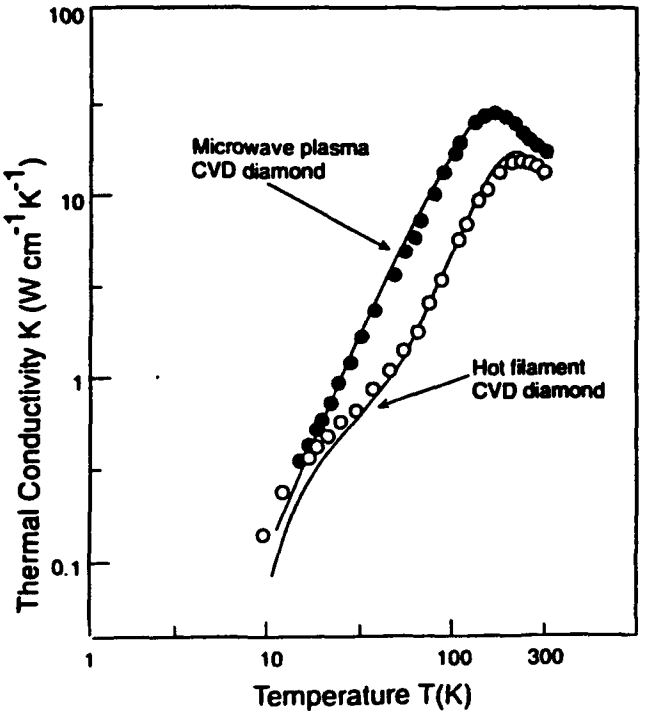

FIGURE 36. Thermal Conductivity of Raytheon CVD Diamond Produced in a Microwave Plasma or Hot-Filament Reactor.

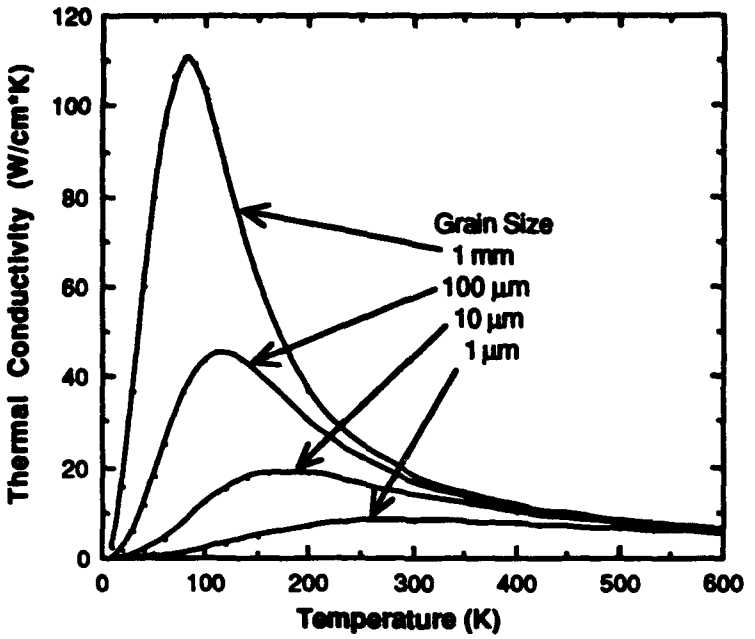

FIGURE 37. Calculated (Reference 22) Thermal Conductivity of Diamond Showing the Effect of Particle Size (Data from C. J. Robinson, Raytheon).

The thermal conductivity of CVD diamond is anisotropic (Reference 26). When measured in the plane of a disk (whose growth direction is normal to the disk) near 300 K, the conductivity of the best Raytheon CVD diamond is 17 to 20 W/(cm·K), which is consistent with that of natural diamond of the same grain size. When measured through the thickness of a disk (parallel to the growth direction), the thermal conductivity is 22-26 W/(cm·K), which is as high as the values reported for Type IIa diamond at 300 K. Norton manufactures several grades of diamond with increasing quality. "Tribology" grade diamond has a conductivity of 6-8 W/(cm·K) measured in the plane of the disk near 300 K. "Thermal management" grade material has a conductivity of 10-12 W/(cm·K) and "optical" grade material has a conductivity of 13-15 W/(cm·K)

From Figure 37 we expect that good quality polycrystalline diamond should have the same thermal conductivity as Type IIa diamond above temperatures of 500 K. For completeness, then, Figure 38 shows the measured conductivity of Type IIa diamond between 500 and 1200 K. We expect that these same values should apply to high quality CVD diamond in this temperature range. (High quality CVD diamond from DeBeers (Reference 27) with a thermal conductivity of 20 W/(cm·K) at 300 K has a conductivity of 12 W/(cm·K) at 480 K, which is similar to Type IIa diamond and shown by the circle in Figure 38.)

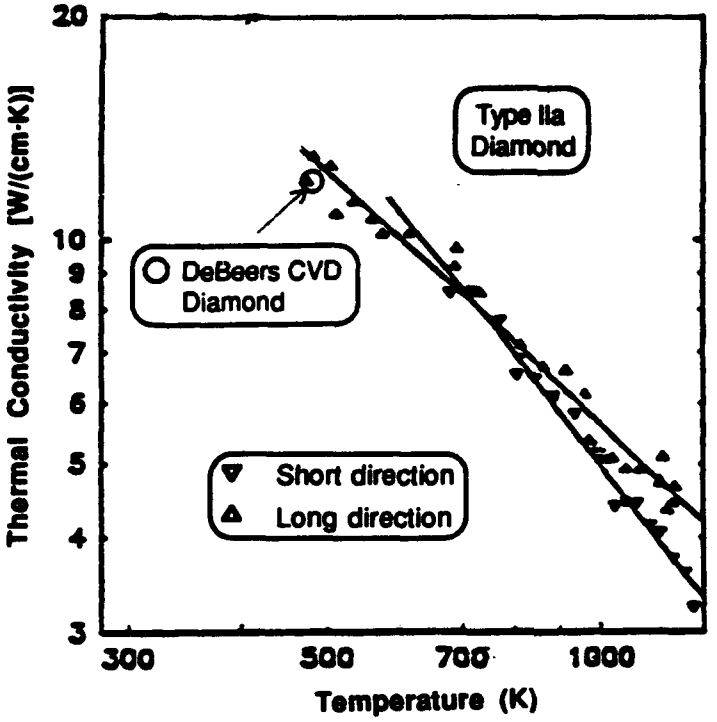

FIGURE 38. Measured Thermal Conductivity of Type IIa Diamond at Elevated Temperature (Reference 28). The sample had dimensions of 8.04 x 8.84 x 2.35 mm. Conductivity measured in the "long direction" refers to the 8.04 mm length. The "short direction" refers to the 2.35 mm length. The circle refers to one specimen of high quality CVD diamond from DeBeers (Reference 27).

A straight line was drawn by hand, going through the data in Figure 38 and through the point (23.4 W/(cm·K) at 300 K). The equation for this line, which we recommend for estimating thermal conductivity (k) of Type IIa or CVD diamond in the range 300-1200 K, is

$$k = \frac{2.833 \times 10^4}{T^{1.245}} \qquad (13)$$

where k has the units W/(cm·K) and T is in kelvins.

MECHANICAL PROPERTIES

HARDNESS, MODULUS, POISSON'S RATIO, AND TOUGHNESS

Hardness measures resistance to indentation and depends on the indentor geometry, the applied load, and the crystal orientation of the material being indented. Diamond is the hardest known material, with a hardness commonly taken to be ~9000 kg/mm^2 (~90 GPa) (References 29 and 30). (This can be compared to values of 4500 for cubic boron nitride, 2000-4000 for silicon carbide and 2000 kg/mm^2 for sapphire.) In two studies, the hardness of CVD diamond was similar to that of natural diamond (References 31 and 32) and dropped by ~30% in the 800-950°C range. (The drop took place between 650 and 800°C.) In another study, four samples had an average hardness of 16 000 kg/mm^2 (~160 GPa) (Reference 33). *Young's modulus and Poisson's ratio for single crystal diamond are*

anisotropic. Appropriate averaging over all orientations predicts a modulus of 1140 GPa and Poisson's ratio of 0.069 for randomly oriented CVD diamond (References 34). These values are consistent with experimental data.

Fracture toughness (K_{Ic}) measures resistance to crack extension. For single crystal diamond, the toughness is estimated to be ~3.4 MPa$\sqrt{m}$ (Reference 35). Indentation measurements on CVD diamond gave a value of 5.3 ±1.3 MPa$\sqrt{m}$ (Reference 36). Fracture surface analysis of biaxial flexure specimens of CVD diamond gave a fracture toughness of 8 ±1 MPa$\sqrt{m}$ (Table 11), while indentation of the same set of samples gave a toughness of 8 ±2 MPa$\sqrt{m}$ (Reference 33). It is normal for polycrystalline materials to have approximately twice the fracture toughness of single crystals.

MECHANICAL STRENGTH

Tables 9-11 list strength measurements made in the present program. Table 12 summarizes the results and compares them to other measurements of CVD diamond strength reported in the literature.

The ring-on-ring test fixture designed for the measurements in Table 9 is shown schematically in Figure 39 (Reference 37). The diamond disk was supported underneath by a Mo ring with a contact radius of 8.61 mm. Load was applied from above through another Mo ring with a contact radius of 4.88 mm. Ti washers with a thickness of 0.076 mm were placed between the fixture and the diamond to reduce the compressive stresses in the diamond normal to the surface at the contact points. Ti was chosen because it could be used for tests up to 1000°C in an Ar atmosphere. For measurements in Table 11, the load was applied at one contact point with a ball instead of a ring (Reference 33).

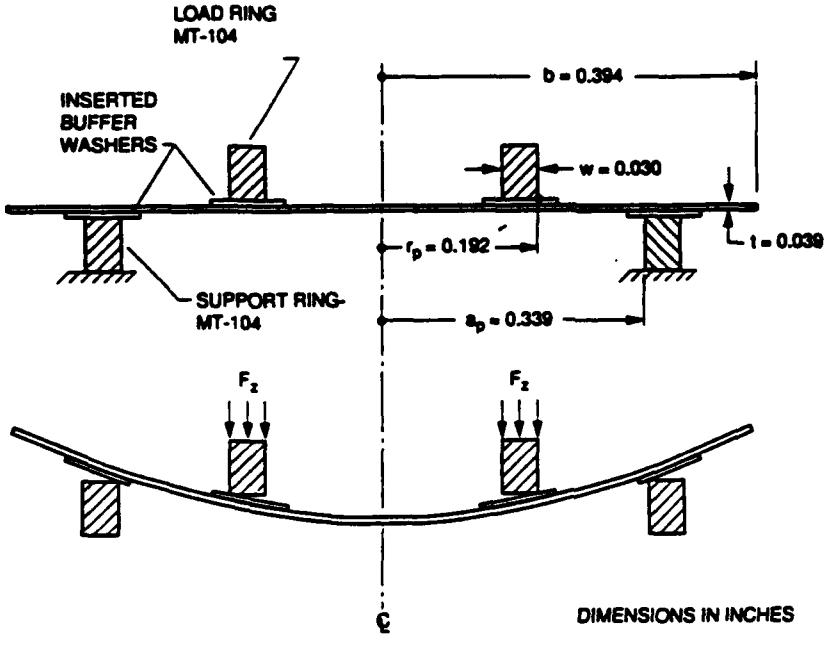

FIGURE 39. Ring-on-Ring Biaxial Flexure Test Fixture for Measuring Strength of Diamond Disks in Table 9 (Reference 37). MT-104 load and support rings are a 99% Mo alloy. Buffer washers are 0.076 mm thick Ti.

TABLE 9. Ring-on-Ring Biaxial Flexure Strength of CVD Diamond Disks Measured at General Research Corp. (Santa Barbara, Calif.)

Specimen	Thickness, mm	Strength, MPa[a]	Tensile face[b]
Norton specimens tested at 20°C			
TD994-03	0.876	136	growth
TD994-04	0.907	136	substrate
TD994-09	0.877	276	substrate
TD994-10	0.892	129	growth
Average TD994		**169 ±71**	
TD1022-15	0.628	285	substrate
TD1022-19	0.628	269	substrate
TD1022-22	0.627	324	growth
Average TD1022		**293 ±28**	
TD1068-26	0.648	463	substrate
TD1068-27	0.640	411	substrate
Average TD1068		**437**	
Norton specimens tested at 1000°C			
TD994-07	0.907	331	substrate
TD1022-18	0.635	318	substrate
TD1068-29	0.503	(157[c]?) 584	substrate
Average		**411 ±150**	
Texas Instruments specimens tested at 20°C			
22D	0.964	281	
22E	1.092	345	
22F	0.894	292	
62A	1.066	188	
73G	1.250	110	
73K	0.866	160	
78B	0.830	140	
Raytheon specimens tested at 20°C			
H155-02	0.834	167	substrate
H155-04	0.824	106	growth
H155-05	0.932	136	substrate
H155-06	0.902	339	growth
H155-10	0.823	161	substrate
H155-12	0.972	159	substrate
H155-13	0.889	149	substrate
H155-14	0.852	183	substrate
H155-19	0.848	224	substrate

[a] Disks with a diameter of 20 mm were tested in ring-on-ring flexure using a 4.88 mm load radius and 8.61 mm support radius (References 37 and 38).

[b] Growth surface is coarse grain surface. Substrate side is fine grain surface.

[c] A sound was heard at the lower strength value, but the sample continued to bear the load until breaking at the higher value.

TABLE 10. Ring-on-Ring Biaxial Flexure Strength of CVD Diamond Disks Measured at Raytheon.[a]

Specimen	Surface treatment	Thickness, mm	Number of samples	Strength, MPa	Tensile face
MP2-51	unpolished	0.24-0.26	4	430 ±150	substrate
MP2-51	unpolished	0.24-0.26	3	189 ±8	growth
MP1-358	unpolished	0.48-0.52	2	420 ±35	substrate
MP1-358	unpolished	0.46-0.51	2	170 ±21	growth
MP2-83	unpolished	0.41	1	490	substrate
MP2-83	abrasion polish	0.35-0.40	4	220 ±20	growth
MP1-339	Fe planarization	0.37-0.41	3	260 ±40	growth

[a] Disks with a diameter of 17 mm were tested in ring-on-ring flexure using a 3.50 mm load radius and 7.00 mm support radius. Crosshead speed = 0.05 cm/min.

TABLE 11. Ball-on-Ring Biaxial Flexure Strength of Texas Instruments CVD Diamond Disks (8 to 15 mm Diameter) Measured at University of Florida.[a]

Crack radius c (μm)	Stress at disk center, MPa	Radial position of fracture	Strength, MPa	Fracture toughness, MPa$\sqrt{m}$	Thickness, mm	Support radius, mm
Unpolished samples						
184 ±18	3220		...		0.59	3.18
43 ±4	1340	370 ±19	970	8	0.39	3.18
87 ±9	820	153 ±8	740	9	0.40	3.18
87 ±9	970	290 ±15	660	8	0.21	3.18
...	110		...		0.66	3.18
...	3600		...		0.043	3.18
...	4030		...		0.042	3.18
...	930		...		0.31	2.48
...	1430		...		0.26	2.48
Polished samples						
42 ±4	1340	194 ±10	720	6	0.19	3.18
107 ±11	1060	215 ±11	680	9	0.22	3.18
103 ±10	1110	303 ±15	650	8	0.30	3.18
37 ±4	910	174 ±9	770	6	0.17	6.35
66 ±7	900	406 ±20	850	9	0.41	3.18
...	1490	...	...		0.19	3.18
...	1310	...	...		0.20	3.18
Averages						
84 ±46	1540 ±1090	...	630 ±260	8 ±1	...	...

[a] Reference 33.

TABLE 12. Comparison of Strength Measurements of CVD Diamond Disks.

Diamond source	Type of test	Thickness, μm	Diameter, mm	Strength, MPa
Norton (Table 10)	ring-on-ring	600-900	20	270 ±120
Norton (Table 10)	ring-on-ring (1000°C)	500-900	20	411 ±150
Texas Instruments (Table 10)	ring-on-ring	800-1200	20	220 ±90
Raytheon (Table 10)	ring-on-ring	800-1000	20	180 ±70
Raytheon (Table 10)	ring-on-ring	240-520	17	~300
Texas Instruments (Table 10)	ball-on-ring	170-410	8-15	630 ±260
Raytheon[a] (9 specimens)	gas burst pressure	4-161	3-11	730 ±350
NEC (Japan)[b] (3 membranes)	gas burst pressure	1.2-2.5	15	1400 ±400
DeBeers[c] (6 specimens)	gas burst pressure	179-300	10-20	900 ±140

[a] Reference 39.
[b] Reference 40.
[c] Reference 41.

Conclusions from Tables 9-12 include the following:

1. Average strengths of CVD diamond from Norton, Texas Instruments and Raytheon tested with a ring-on-ring fixture are in the approximate range 200-400 MPa. These strengths are approximately 1/10 of the ~3 GPa tensile strength quoted for natural diamond (Reference 42). (Bear in mind that it is difficult to measure the strength of small single crystals of diamond and results are not directly comparable to results from flexure tests of disk.)

2. The strength of currently available CVD diamond at 1000°C is not lower than the strength at 20°C. (It is possible that higher strength material produced in the future could lose strength at elevated temperature.)

3. The strengths of the three different sets of Norton diamond in Table 9 (from growth runs TD994, TD1022, and TD 1068) appear to be different from each other. Each of these growth runs was uniform in appearance and the limited strength data are also reasonably uniform with each set. This observation suggests that under some conditions stronger diamond can be grown.

4. In Table 9, there was no difference in tensile strength between the substrate (fine grain, Figure 16) and growth (coarse grain, Figure 17) surfaces of polished CVD diamond. In Table 10 the substrate surface is about twice as strong as the growth surface.

5. Ball-on-ring flexure strengths in Table 11 are significantly greater than the ring-on-ring strengths in Tables 9 and 10. This typical result for ceramics arises because the ball-on-ring test places less volume or area under stress than the ring-on-ring test.

6. The strengths of thin disks of Raytheon CVD diamond tested by pressurizing one side with gas (third line from the bottom in Table 12) are somewhat higher than the strengths of thick disks. The thinnest specimen (4 μm thick) had the greatest strength (1380 MPa). This is not surprising because a thin membrane cannot have critical flaws that are as deep as a thick disk.

7. The strengths of very thin (1.2 to 2.5 μm) diamond membranes (second line from the bottom in Table 12) are more than 1 GPa. As stated in conclusion 6, thin membranes cannot have deep flaws, so they are expected to be strong.

8. The burst strength of DeBeers diamond at the bottom of Table 12 is greater than the strengths of the disks in Tables 9 through 11. We do not know if this means that the DeBeers diamond is really stronger or if the different test conducted by DeBeers gives a systematically higher result than the ring-on-ring test. Depending on the effective constraint at the edge of the DeBeers disks during flexure, the stress state ranges from maximum at the center, to fairly uniform across the disk, to maximum at the edges. We do not know how to compare the DeBeers strength to ours. The DeBeers disks were only one third as thick as those in Table 9, so the critical flaw sizes were probably not as great. Before concluding that DeBeers diamond is any stronger than Norton, Raytheon, or Texas Instruments diamond, it is necessary to test DeBeers diamond with a thickness near 1 mm in a ring-on-ring fixture.

9. In the DeBeers study, three pieces of single-crystal silicon (thickness = 0.53 mm, diameter = 10 mm) had an average strength of 150 ±30 MPa, when subjected to the same test as diamond. One specimen of single-crystal sapphire (thickness = 0.58 mm, diameter = 20 mm) had a strength of 405 MPa. Comparison of the DeBeers diamond strength to the silicon and sapphire strength suggests that DeBeers diamond may really be stronger than sapphire.

Figure 40 shows the fracture patterns of Norton diamond disks from Table 9. Stronger brittle materials, in general, shatter into more pieces than weaker samples of the same material. In comparison to fracture patterns observed in zinc sulfide and sapphire, the diamond in Figure 40 represents relatively weak material. This gives us hope that there is room for improvement.

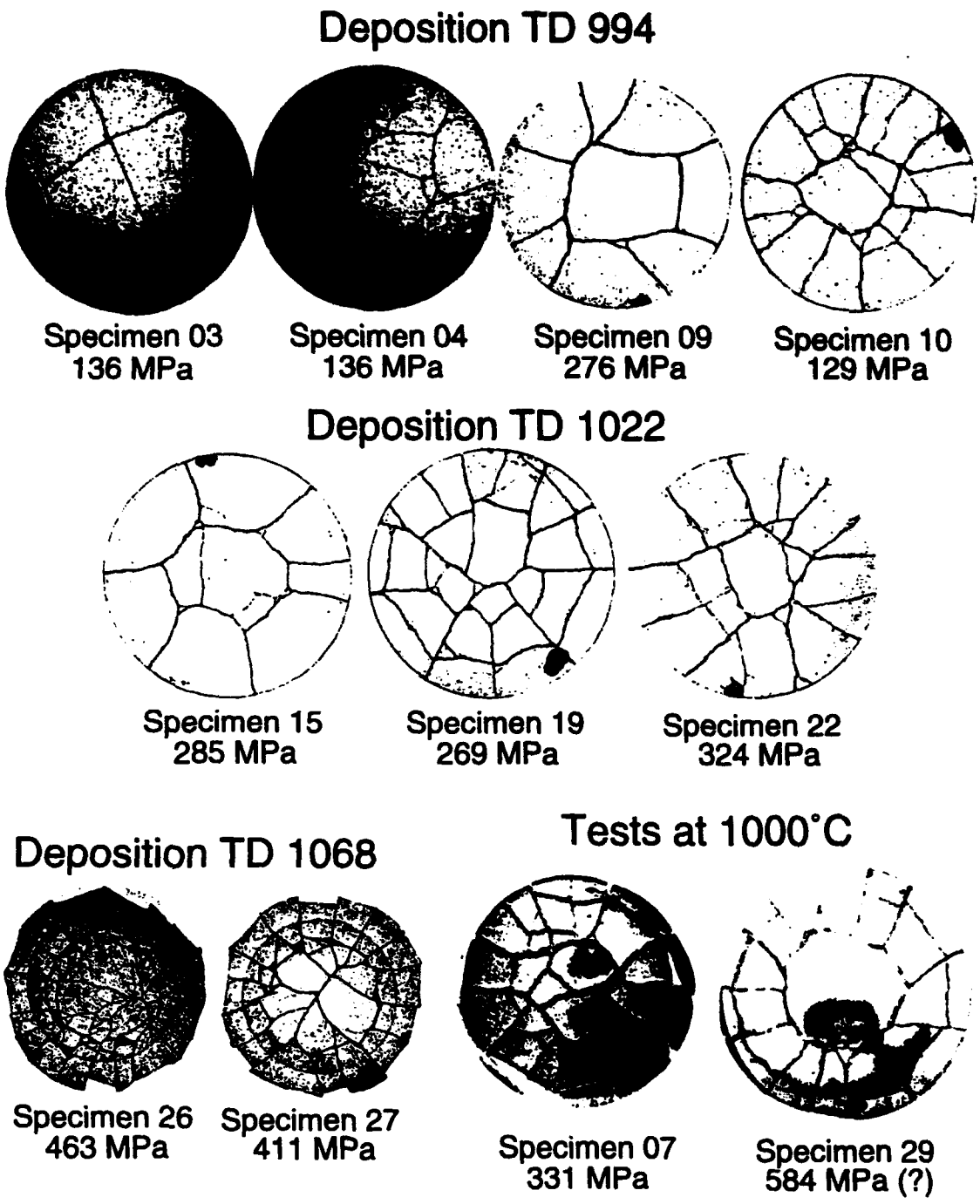

FIGURE 40. Fracture Patterns of Norton Diamond Disks From Table 9 (Reference 37).

THE STRENGTH OF DIAMOND IS GOVERNED BY FLAW SIZE

The strength of brittle materials is related to the size of pre-existing flaws by the equation

$$\text{Strength} = \frac{K_{Ic}}{1.24\sqrt{c}} \tag{14}$$

where K_{Ic} is the fracture toughness and c is the radius of the critical flaw that gives rise to fracture. (For elliptical flaws with radii a and b, $c = \sqrt{ab}$.) It is rather difficult (and takes some imagination) to find the critical flaws in broken pieces of polycrystalline diamond. Figure 41 shows an example of a fracture origin identified by characteristic river marks leading away from the origin. Table 11 shows that K_{Ic} calculated from the measured strength and crack radius is constant near 8 MPa$\sqrt{m}$ for 8 specimens. That is, the strength of CVD diamond is governed by flaws. If the flaws were smaller, the strength would be greater. The average length of a critical flaw in Table 11 is $2c \approx 170$ μm. If the flaw size were reduced by a factor of 4, the strength would increase by a factor of 2.

How big are the critical flaws in natural diamond? If we take the strength of natural diamond as 3 GPa and the fracture toughness as 3.4 MPa$\sqrt{m}$, Equation 14 tells us that the flaw size is $2c = 1.6$ μm.

Flaws that may serve as fracture origins are readily observed under a microscope everywhere in any piece of CVD diamond. Figures 23, 24 and 26 showed some examples of flaws. Figure 42 shows cracks radiating into a single grain, suggesting that the diamond was under extreme stress at some time. Figure 43 shows a void that was apparently buried inside the growing diamond.

FINE POLISHING HAS NO EFFECT ON THE STRENGTH OF DIAMOND (YET)

Optical ceramics typically contain few buried critical flaws. These materials generally fail in tension from surface flaws such as polishing scratches. An experiment was carried out to see if strength might be limited by scratches introduced in the very aggressive abrasive polishing of diamond with fine diamond grit. Diamond from Norton growth run TD 1068 was laser cut into 8-mm-diameter disks and sent to Edge Technologies (Indianapolis, Ind.) for a proprietary, nonabrasive chemical polishing that produced a root-mean-square surface roughness of 7 nm. One large abrasively polished disk from this same growth run was laser cut into three 8-mm-diameter disks. The growth side had a roughness of 44 nm and the substrate side had a roughness of 18 nm. Nomarski microscopy showed that the chemically polished diamond had a much smoother surface with many fewer defects than the abrasively polished diamond (Figure 44). The flexure strengths of both sets of disks in Table 13 was similar, showing that the less destructive chemical polish had no effect on strength. We conclude that strength is limited by flaws that are so prevalent that surface quality is not yet relevant.

FIGURE 41. Fracture Surface of Polycrystalline Diamond (Norton disk 30C), With an Outline Around the V-Shaped Critical Flaw. Characteristic "river marks" on either side of the fracture origin point toward the origin. Magnification of the upper photo is ~100× (Figure and interpretation courtesy of J. J. Mecholsky, Jr. and L. Hehn, University of Florida).

FIGURE 42. *Upper*: Reflection Optical Micrograph of the Surface of Raytheon CVD Diamond Specimen 294B. *Lower:* Transmission optical micrograph of the same grain seen in the upper figure, focused 38 µm into the growth surface. Cracks are seen radiating into the grain from its edges.

FIGURE 43. Laser Cut of Raytheon CVD Diamond Exposes a Buried Void. Marker bar is 100 μm.

TABLE 13. Strength of Abrasively-Polished and Chemically Polished Diamond Disks.[a]

Specimen	Stress at center, MPa	Stress at failure origin, MPa	Critical flaw radius, μm	Fracture toughness K_{Ic}, MPa$\sqrt{m}$
Abrasive polish				
TD1068-30A	637	637	110	8.3
TD1068-30B	631	631	121	8.6
TD1068-30C	682	653	104	8.3
Chemical polish				
TD1068-38	628	628	114	8.3
TD1068-40	639	390	147	5.9

[a] CVD Diamond disks (8 mm diameter x 0.64 mm thick) with substrate surface in tension. Ball-on-ring fixture with 3.2 mm diameter support ring.

WATERJET IMPACT RESISTANCE

A primary reason for using a diamond optical window is to increase durability with respect to damage by sand and rain. Natural diamond is unsurpassed in its erosion resistance. For example, natural diamond impacted by sand at 26 m/s suffered a mass loss that was 20 000 times less than the rate of mass loss from silicon nitride impacted at 47 m/s (Reference 43). Static indentation of 6-15 μm-thick diamond films with a tungsten carbide ball gave characteristic ring cracks from which the tensile strength of the film was estimated to be 1.4 GPa (Reference 44). Natural diamond in the same test has a strength of 4-6 GPa.

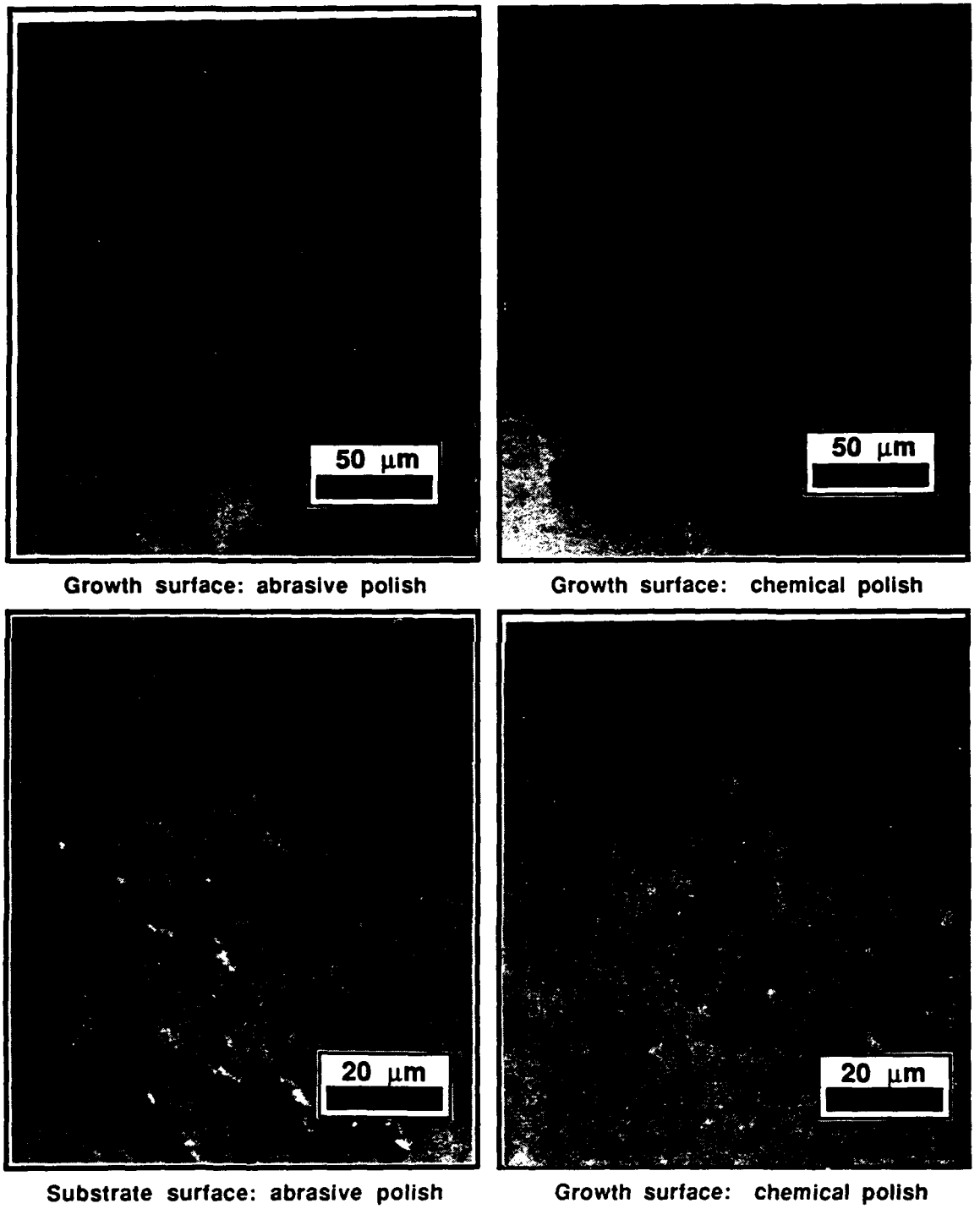

FIGURE 44. Nomarski Micrographs of Growth (360×) and Substrate Surfaces (900×) of Abrasively and Chemically Polished CVD Diamond From Norton Growth Run TD 1068.

Figure 45 shows that Type IIa diamond has the highest waterjet damage threshold velocity of any infrared window material (Figure 45) (References 44 through 46). In this experiment, the 1-mm-thick x 6-mm-diameter single specimen of natural diamond (fully supported on an x-y stage) was impacted by a jet of water from a 0.8-mm-diameter nozzle. There was no damage visible under a microscope after many impacts at velocities below 530 m/s (equivalent to ~600 m/s for a 2-mm-diameter waterdrop). After 170 impacts at 530 m/s, the sample shattered. For comparison, two samples of single crystal sapphire exhibited microscopically visible damage at threshold velocities near 430 m/s (equivalent to ~535 m/s for a 2-mm-diameter waterdrop). It was speculated (Reference 44) that the damage threshold velocity for thicker diamond might be even greater than 530 m/s because the thin specimen may experience damage from waves reflected from the back surface of the sample.

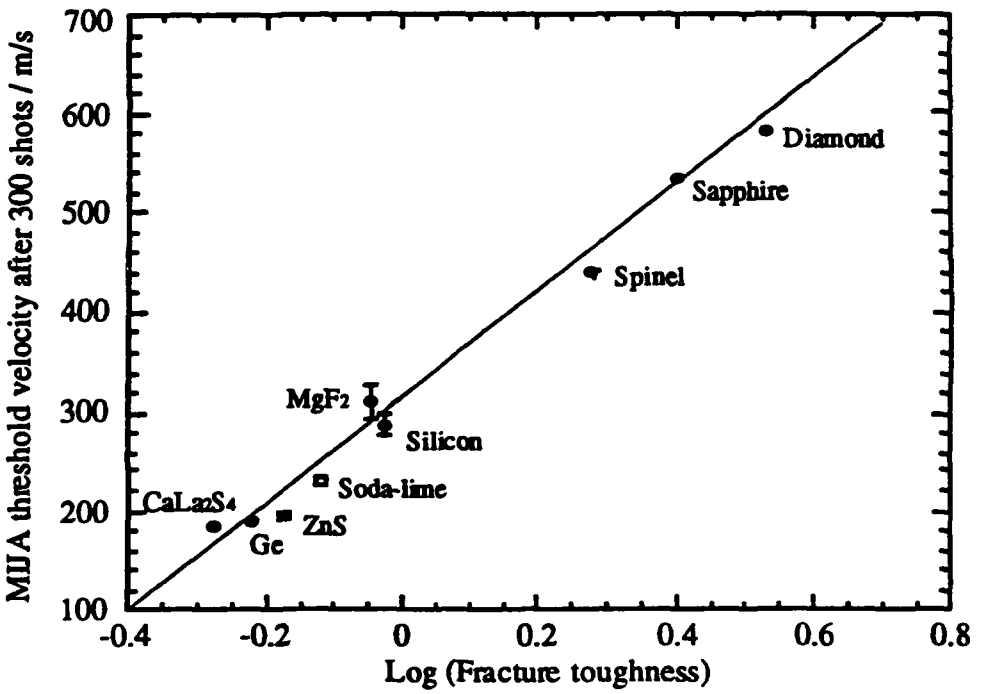

FIGURE 45. Waterjet Damage Threshold Velocity of Infrared Window Materials Tested With a Multiple Impact Jet Apparatus Scales With the Logarithm of the Indentation Fracture Toughness (Reference 45). Velocities in this figure are "corrected" to be equivalent to those of 2-mm-diameter waterdrops. The actual damage threshold velocity of the waterjet (from a 0.8 mm nozzle) was 430 m/s for sapphire and ~530 m/s for diamond.

Figure 46 gives one example of the results of waterjet impact on a 0.9-mm-thick sample of CVD diamond. Central crazing (located ~200 μm below the surface of the sample) was first observed after 10 impacts at 250 m/s, and it increased in extent with repeated impacts at higher velocities. Central crazing is not usually observed with other ceramics, and may be caused by the large population of pre-existing microcracks in CVD diamond. Circumferential cracking was first noted after 10 impacts at 500 m/s. The diameter of the circumferential crack is ~4 times larger than would be observed in ZnS, and

might be due to stress wave reflection from the back surface of the sample reinforcing Rayleigh waves on the impacted surface.

CVD diamond specimens 5 and 29 from Norton, H155-18 from Raytheon, and NW2-62C from Texas Instruments all behaved in a similar manner. Norton sample 29 came from Growth Run TD 1068 that had higher optical quality and higher average strength than Growth Run TD 994 that produced specimen 5. Yet disk 29 had lower damage threshold velocities than disk 5. Central crazing was observed after 10 impacts at 200 to 250 m/s and circumferential cracking after 10 impacts at 350 to 400 m/s.

Norton site # 4 - after 20 impacts at 500 m s^{-1}

Central damage appeared after 10 impacts at 250 m s^{-1}
Circumferential cracking after 10 impacts at 500 m s^{-1}

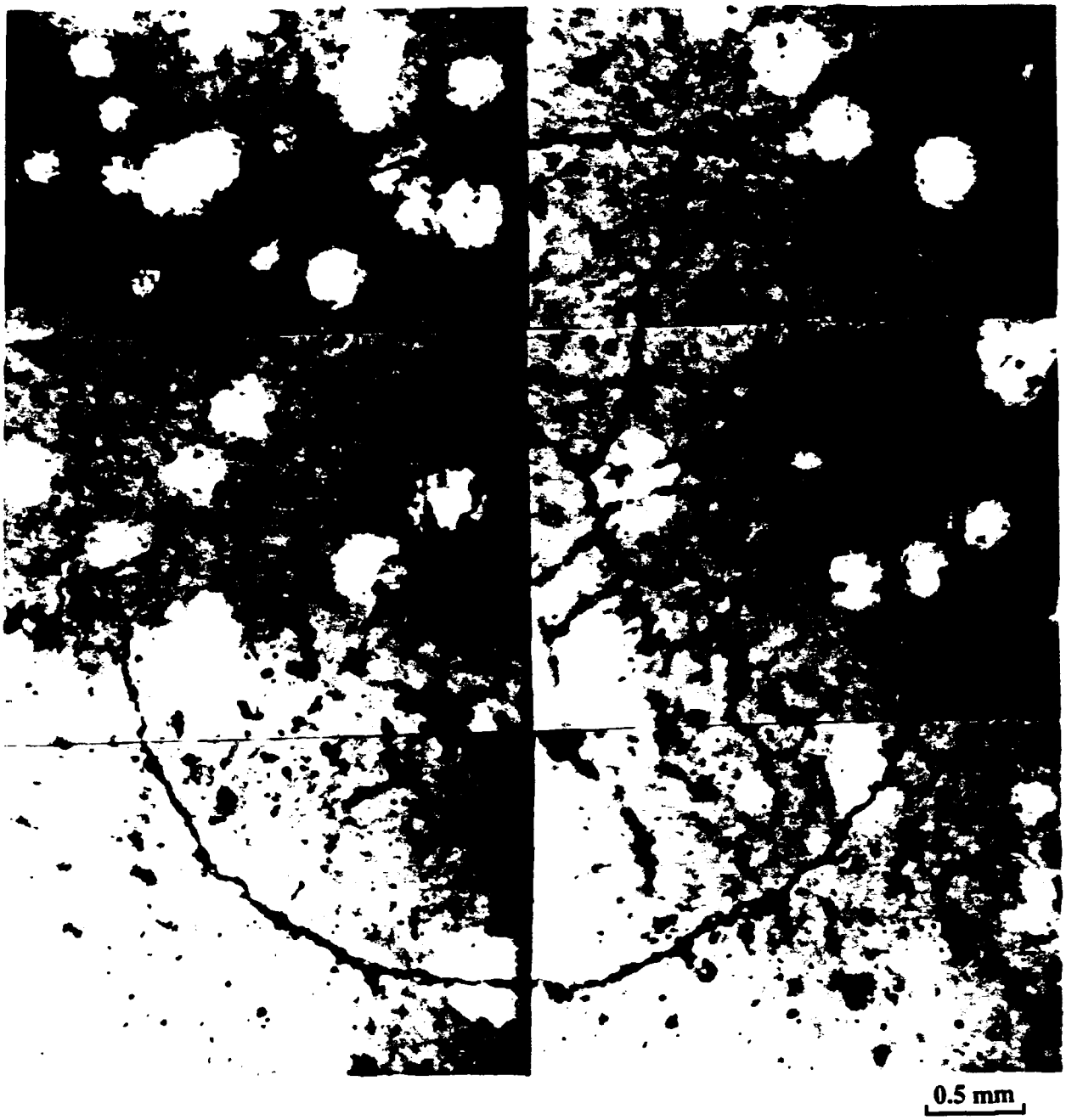

Plate 3.7.1 Photo of site after 20 impacts at 500 m s^{-1}

FIGURE 46. Waterjet Damage Site on Substrate Side of Polished CVD Diamond Disk Number 5 From Norton (Reference 45). Central crazing is located ~200 μm below the impacted surface. The ring fracture is on the surface.

REFERENCES

1. R. D. Clay and J. P. Clay, *Proc. SPIE, 505* (1984), p. 57.

2. Naval Air Warfare Center Weapons Division. *Materials for 2-Color Infrared Domes for High-Speed Missiles*, by D. C. Harris and P. E. Bunting. China Lake, Calif., NAWCWPNS, July 1993. (NAWCWPNS TP 8129, publication UNCLASSIFIED).

3. C. E. Johnson, M. A. S. Hasting, and W. A. Weimer, *J. Mater. Res., 5* (1990), p. 2320; C. E. Johnson, W. A. Weimer, and D. C. Harris, *Mat. Res. Bull., 24* (1989), p. 1127.

4. M. Seal, *Nature, 182* (1958), p. 1264; M. Seal, *Nature, 185* (1960), p. 522; T. Evans and P. F. James, *Proc. Roy. Soc. Lond., A277* (1964), p. 260; G. Davies and T. Evans, *Proc. Roy. Soc. Lond., A328* (1972), p. 413.

5. S. Jin, J. E. Graebner, G. W. Kammlott, T. H. Tiefel, S. G. Kosinski, L. H. Chen, and R. A. Fastnacht, *Appl. Phys. Lett., 60* (1992), p. 1948; S. Jin, J. E. Graebner, M. McCormack, T. H. Tiefel, A. Katz, and W. C. Dautremont-Smith, *Nature, 362* (1993) p. 822.

6. K. Tankala, T. Debroy, W. A. Yarbrough, and C. J. Robinson, *Diamond and Related Materials, 1* (1992), p.1177.

7. C. A. Klein, T. M. Hartnett and C. J. Robinson, *Phys. Rev. B, 45* (1992), p. 12854.

8. K. M. McNamara, D. H. Levy, K. K. Gleason, and C. J. Robinson, *Appl. Phys. Lett., 60* (1992), p. 580.

9. J. M. Trombetta, J. T. Hoggins, P. Klocek, and T. A. McKenna, *Proc. SPIE* 1991, *1534*, p. 77.

10. Oak Ridge National Laboratory/Army Space and Strategic Defense Command. *High Temperature Optical Characterization of CVD Diamond and Natural Type IIa Diamond*, by R. E. Clausing, J. R. McNeely, M. B. McIntosh, W. B. Snyder, Jr., M. E. Thomas, M. J. Linevsky, and W. J. Tropf. Oak Ridge, Tenn., 31 October 1992. (MMES/USASDC/SDIO/TP-92-12, publication UNCLASSIFIED.)

11. Johns Hopkins University Applied Physics Laboratory. *Temperature Dependent Transmittance and Reflectance Measurements on Natural Type IIa and CVD Diamond Windows*, by M. E. Thomas. Laurel, Md., JHU/APL, 30 December 1993. (JHU/APL Memorandum F1F(4)93-U-282, publication UNCLASSIFIED.)

12. M. E. Thomas and W. J. Tropf, *Johns Hopkins APL Technical Digest, 14* (1) (1993), p. 16.

13. K. Harris, G. L. Herrit, C. J. Johnson, S. P. Rummel, and D. Scatena, *Appl. Opt., 30* (1991), p. 5015; *Ibid., 32* (1992), p. 4342.

14. I. Kiflawi, C. M. Welbourn and G. S. Woods, *Solid State Commun., 85* (1993), p. 551.

15. J. C. Stover, *Proc. SPIE, 1326* (1990), p. 321.

16. P. C. Archibald and H. E. Bennett, *Opt. Eng., 17* (1978), p. 647.

17. E. D. Palik, ed. *Handbook of Optical Constants of Solids*, Boston, Academic Press, 1985.

18. J. Fontanella, R. L. Johnston, J. H. Colwell, and C. Andeen, *Appl. Opt., 16* (1977), p. 2949.

19. M. H. Grimsditch, E. Anastassakis, and M. Cardona, *Phys. Rev. B, 18* (1978), p. 901; H. Boppart, J. van Straaten, and I. F. Silvera, *Phys. Rev. B, 32* (1985), p. 1423; S. K. Sharma, H. K. Mao, P. M. Bell, and J. A. Xu, *J. Raman Spec., 16* (1985), p. 350.

20. J. Wagner, C. Wild, and P. Koidl, *Appl. Phys. Lett., 59* (1991), p. 779.

21. L. H. Merwin, C. E. Johnson, and W. A. Weimer, *J. Mater. Res., 9* (1994), p. 631.

22. C. J. Robinson, T. M. Hartnett, R. P. Miller, C. B. Willingham, J. E. Graebner, and D. T. Morelli, *Proc. SPIE, 1739* (1993), p. 146.

23. D. T. Morelli, C. Uher, and C. J. Robinson, *Appl. Phys. Lett., 62* (1993), p. 1085.

24. D. T. Morelli, T. M. Haretnett, and C. J. Robinson, *Appl. Phys. Lett., 59* (1991), p. 2112.

25. D. J. Pickrell, K. A. Kline, and R. E. Taylor, *Appl. Phys. Lett., 64* (1994), p. 2353.

26. J. E. Graebner, S. Jin, G. W. Kammlott, B. Bacon, L. Seibles, and W. Banholzer, *J. Appl. Phys., 71* (1992), p. 5353.

27. C. J. H. Wort, C. G. Sweeney, M. A. Cooper, G. A. Scarsbrook, and R. S. Sussman "Thermal Properties of Bulk Polycrystalline CVD Diamond," Diamond '93 Conference, Portugal, September 1993.

28. J. W. Vandersande, C. B. Vining, and A. Zoltan, *NASA Technical Brief*, Vol. 16, No. 12, Item #5, December 1992.

29. J. E. Field. *The Properties of Natural and Synthetic Diamond*, London, Academic Press, 1992. Chap. 13 and p. 674.

30. C. A. Brookes and E. J. Brookes, *Diamond and Related Materials, 1* (1991), p. 13.

31. D. R. Mumm, K. T. Faber, M. D. Drory, and C. F. Gardinier, *J. Am. Cer. Soc., 76* (1993), 238.

32. C. J. McHargue. "Mechanical Properties of Diamond and Diamond-Like Films," in *Applications of Diamond Films and Related Materials*, ed. by Y. Tzeng, M. Yoshikawa, M. Murakawa, and A. Feldman, Amsterdam , Elsevier, 1991.

33. L. P. Hehn, Z. Chen, J. J. Mecholsky, Jr., P. Klocek, J. T. Hoggins, and J. M. Trombetta, *J. Mater. Res., 9* (1994), in press.

34. C. A. Klein, *Mater. Res. Bull., 27* (1992), p. 1407; C. A. Klein and G. F. Cardinale, *Diamond and Related Materials, 2* (1992), p. 918.

35. J. E. Field. *The Properties of Natural and Synthetic Diamond*, London, Academic Press, 1992. Chap. 12.

36. M. D. Drory, C. F. Gardinier, and J. S. Spek, *J. Am. Cer. Soc., 74* (1991), p. 3148.

37. General Research Corporation. *Biaxial Flexure Testing of Diamond Disks*, by W. F. Adler, D. J. Mihora, and J. W. Flavin. Santa Barbara, Calif., GRC, 31 December 1993. (GRC Report CR-93-1366, publication UNCLASSIFIED.)

38. General Research Corporation. *Biaxial Flexure Testing and Waterdrop Impact Testing of Diamond Disks*, by W. F. Adler, J. W. Flavin, and J. P. Richards. Santa Barbara, Calif., GRC, 31 December 1993. (GRC Report CR-93-1372, publication UNCLASSIFIED.)

39. G. F. Cardinale and C. J. Robinson, *J. Mater. Res., 7* (1992), p. 1432.

40. Y. Aikawa and K. Baba, *Jap. J. Appl. Phys., 32* (1993), p. 4680.

41. T. J. Valentine, A. J. Whitehead, R. S. Sussman, C. J. H. Wort, and G. A. Scarsbrook, "Mechanical Property Measurement of Bulk Polycrystalline CVD Diamond," Diamond '93 Conference, Portugal, September 1993.

42. J. E. Field. *The Properties of Natural and Synthetic Diamond*, London, Academic Press, 1992. P. 679 and Chap. 12.

43. I. P. Hayward and J. E. Field, *J. Hard Mater., 1* (1990), p. 53.

44. C. R. Seward, C. J. S. Pickles, J. E. Field, and Z. Feng, *Diamond and Related Materials, 2* (1993), p. 606; Z. Feng, Y. Tzeng, and J. E. Field, *Thin Solid Films, 212* (1992), p. 35.

45. C. R. Seward, E. J. Coad, and J. E. Field, *The Rain Erosion Resistance of CVD Diamond*, Contract No. 2029/262/DCVD, Cavendish Laboratory, University of Cambridge, October 1993.

46. C. R. Seward, C. J. S. Pickles, R. Marrah, and J. E. Field, *Proc. SPIE, 1760* (1992), p. 280.

INITIAL DISTRIBUTION

2 Naval Air Systems Command, Arlington
  AIR-5166M, R. Retta (1)
  AIR-540TB, P. Facas (1)
2 Naval Sea Systems Command, Arlington
  PMS-422-1, B. Lubin (1)
  SEA-06KRb, D. Muir (1)
8 Office of Naval Research, Arlington
  ONR-314, M. Yoder (1)
  ONR-331
    H. Guard (1)
    L. Kabacoff (1)
    J. Pazik (1)
  ONR-332
    S. Fishman (1)
    B. Pohanka (1)
    L. Sloter (1)
  ONR-351, D. Siegel (1)
1 Naval Air Warfare Center, Aircraft Division, Indianapolis (MS 36, J. Sosniak)
1 Naval Air Warfare Center, Aircraft Division, Lakehurst (Code 5321, J. Koeppel)
1 Naval Air Warfare Center, Aircraft Division, Warminster (Code 5011, M. Wilson)
1 Naval Command Control and Ocean Surveillance Center, RDTE Division, San Diego (Code 551, P. Sullivan)
2 Naval Research Laboratory
  Code 6174, J. Butler (1)
  Code 6522, K. Snail (1)
1 Naval Surface Warfare Center, Dahlgren Division, Dahlgren (Code R35, C. Blackmon)
4 Naval Surface Warfare Center, Dahlgren Division, White Oak Detachment, Silver Spring
  Code K205, B. Messick (1)
  Code R31, I. Talmy (1)
  Code R33, S. Dallek (1)
  Code R43, K. Hathaway (1)
3 Army Missile Command, Redstone Arsenal
  AMSMI-RD-AS-OG, G. Hutcheson (1)
  AMSMI-RD-SE-MT, B. Park (1)
  AMSMI-RD-ST-CM, S. Patterson (1)
6 Army Space and Strategic Defense Command, Huntsville
  CSSD-KE-E
    R. Calhoun (1)
    T. Street (1)
  CSSD-KE-I, G. Jones (1)
  CSSD-SL-K, G. Lowe (1)
  SFAE-MD-ARW, D. Perry (1)
  SFAE-MD-THA, D. R. McClure (1)
1 Army Research Laboratory/Materials Directorate, Watertown (AMSRL-MA-B, F. Meyer)
1 Army Research Office, Durham (SLCRO-MS, J. Prater)
2 Center for Night Vision and Electronic Sensors Directorate, Fort Belvoir
  AMSEL-RD-NV-IRT, L. J Mizerka (1)
  AMSEL-RO-NV-SO, J. Hall (1)
2 Wright Laboratory, Armament Directorate, Eglin Air Force Base
  WL/MNG, E. Boudreaux (1)
  WL/MNGA, R. Porter (1)

3 Wright Laboratory, Dynamics Directorate, Wright-Patterson Air Force Base
WL/MLPO
R. Denison (1)
R. Ondercin (1)
R. Susnik (1)
1 Advanced Research Projects Agency, Arlington (ARPA/DSO, B. Barker)
1 Ballistic Missile Defense Organization (BMDO/DTI, LTCOL M. Obal)
2 Institute of Defense Analyses Management Office, Alexandria
C. F. Bersch (1)
J. Sater (1)
1 Office of Secretary of Defense (OSD/BMDO, L. H. Caveny)
1 National Institute of Standards and Technology, Gaithersburg, MD (A. Feldman)
1 Oak Ridge National Laboratory, Oak Ridge, TN (R. E. Clausing)
1 Ares Corporation, Arlington, VA (J. Siewick)
1 AsTex, Incorporated, Woburn, MA (D. K. Smith)
1 Auburn University, Auburn, AL (Department of Electrical Engineering, T. Tzeng)
1 Battelle Pacific Northwest Laboratory, Richland, WA P. Martin)
1 California Institute of Technology (Caltech), Pasadena, CA (D. Goodwin)
1 California Institute of Technology (Jet Propulsion Laboratory, Pasadena, CA
(C. R. Lewis)
1 Chuck Wyman, Huntsville, AL
1 Crystallume, Menlo Park, CA (B. Philips)
2 General Electric Company, Schenectady, NY
T. R. Anthony (1)
C. Spiro (1)
1 General Motors Research Laboratories, Warren, MI (Physical Chemistry Department,
S. J. Harris)
1 General Research Corporation, Santa Barbara, CA (B. Adler)
1 Harris Diamond Corporation, Mount Arlington, NJ (K. Harris)
1 Hughes Danbury Optical Systems, Incorporated, Danbury, CT (J. Askinazi)
1 Hughes Missile Systems Company/Pomona, Pomona, CA (J. Winderman)
1 Lockheed Missile and Space Company, Incorporated, Huntsville, AL (C. Wojciechoski)
2 Lockheed Missile and Space Company, Incorporated, Sunnyvale, CA
R. Lim (1)
K. V. Ravi (1)
2 Loral Vought Systems Corporation, Dallas, TX
R. C. Knight (1)
S. Smith (1)
3 Martin-Marietta Missile Systems, Orlando, FL
T. Bailey (1)
J. Meredith (1)
R. Twedt (1)
1 Materials Systems, Incorporated, Littleton, MA (R. Gentilman)
1 McDonnell-Douglas Corporation, Huntington Beach, CA (H. Morris)
2 Morton/CVD, Woburn MA
H. Desai (1)
J. Goela (1)
1 Norton Diamond Films, Northboro, MA (K. Gray)
1 Osram-Sylvania, Danvers, MA (G. Wei)
1 Pennsylvania State University, University Park, PA (W. Yarbrough)
4 Raytheon Company, Research Division, Lexington, MA
L. Goldman (1)
T. Harnett (1)
R. Tustison (1)
C. Willingham (1)
1 Raytheon Company, Missile Systems Division, Tewksbury, MA (P. Boland)
2 Rockwell International Corporation, Rocketdyne Division, Canoga Park, CA
S. Holly (1)
D. Koumvakalis (1)
1 Rockwell International Corporation, Tactical Systems Division, Duluth, GA
(E. L. Fleeman)
1 Rockwell International Science Center, Thousand Oaks, CA (A. Harker)
1 Santa Barbara Research Center, Goleta, CA (R. Hudyma)
1 Stanford University, Palo Alto, CA (M. Cappelli)

1 Strategic Analysis, Arlington, VA (L. Miller)
1 Teledyne Brown, Huntsville, AL (G. Tanton)
3 The Johns Hopkins University, Applied Physics Laboratory, Laurel, MD
  K. Frazer (1)
  M. Thomas (1)
  B. Tropf (1)
3 Texas Instruments, Dallas, TX
  J. Hoggins (1)
  P. Klocek (1)
  J. Trombetta (1)
1 University of Dayton Research Institute, Dayton, OH (J. Detrio)
1 University of Florida, Gainesville, FL (J. J. Mecholsky)
1 Westinghouse Electro-optical Systems, Orlando, FL (B. Cashion)
1 Westinghouse Science and Technology Center, Pittsburg, PA (B. Witkowski)
1 W. J. Schafer Associates, Arlington, VA (C. Byvik)
1 W. J. Schafer Associates, Dayton, OH (D. Evans)
2 BNR Europe Limited, United Kingdom
  R. Heiniche (1)
  I. Llewellyn (1)
3 Cavendish Laboratory, United Kingdom
  J. E. Field (1)
  J. Pickles (1)
  C. Seward (1)
1 Defence Research Agency, United Kingdom (J. A. Savage)